The Determination of $ClNO_2$ via Thermal Dissociation-Tunable Infrared Laser Direct Absorption Spectroscopy

John W. Halfacre[1], Lewis Marden[1], Marvin D Shaw[1], Lucy J Carpenter[1], Emily Matthews[2], Thomas J. Bannan[2], Hugh Coe[2,3], Scott C. Herndon[4], Joseph R. Roscioli[4], Christoph Dyroff[4], Tara I. Yacovitch[4], Patrick R. Veres[5*], Michael Robinson[5,6], Steven S. Brown[5,7], Pete M. Edwards[1,8]

[1]Wolfson Atmospheric Chemistry Laboratories, Department of Chemistry, University of York, Heslington, York, YO10 5DD, UK

[2]Department of Earth and Environmental Science, Centre for Atmospheric Science, School of Natural Sciences, The University of Manchester, Manchester M13 9PL, UK

[3]National Centre for Atmospheric Science, University of Manchester, Manchester, UK

[4]Aerodyne Research, Inc., Billerica, MA, 01821, USA

[5]Chemical Sciences Laboratory, National Oceanic and Atmospheric Administration, Boulder, CO, 80305, USA

[6] Cooperative Institute for Research in Environmental Sciences, University of Colorado, Boulder, CO, 80305, USA

[7]Department of Chemistry, University of Colorado, Boulder, CO 80309, USA

[8]National Centre for Atmospheric Science, University of York, York, UK

*Now at National Science Foundation, National Center for Atmospheric Research, Boulder, CO, 80301, USA

Correspondence to: John Halfacre (john.halfacre@york.ac.uk), Pete Edwards (pete.edwards@york.ac.uk)

Abstract. Nitryl chloride ($ClNO_2$) is a reservoir species of chlorine atoms and nitrogen oxides, both of which play important roles in atmospheric chemistry. To date, all ambient $ClNO_2$ observations have been obtained by chemical ionization mass spectrometry (CIMS). In this work, Thermal Dissociation Tunable Infrared Laser Differential Absorption Spectrometer (TD-TILDAS) is shown to be a viable method for quantifying $ClNO_2$ in laboratory and field settings. This technique relies on the thermal dissociation of $ClNO_2$ to create chlorine radicals, which undergo fast reactions with hydrocarbons to produce hydrogen chloride (HCl) that is detectable by the TILDAS instrument. Complete quantitative conversion of $ClNO_2$ to HCl was achieved at temperatures > 400°C, achieving 1 Hz measurement precision of 11 ± 1 pptv (3σ limits of detection of 34 ± 2 pptv) during laboratory comparisons with other $ClNO_2$ detection methods. After blank- and line loss-corrections, method accuracy is estimated to be within ± 5%. Performance metrics of TD-TILDAS during ambient sampling were a 1Hz precision of 19 ± 1 pptv and 3σ limits of detection of 57 ± 3 pptv), which is directly comparable to previously reported $ClNO_2$ detection by quadrupole CIMS. Thus, TD-TILDAS can provide an alternative analytical approach for a direct measurement of $ClNO_2$ that can complement existing datasets and future studies. The quantitative nature of TD-TILDAS also makes it a potentially useful tool for the calibration of CIMS instruments. However, interpretation of ambient data may be complicated by potential interferences from unaccounted-for sources of thermolabile chlorine, such as ClNO, chloramines, and organochlorides.

1 Introduction

Nitryl chloride ($ClNO_2$) is an important nighttime reservoir of two highly reactive atmospheric species: atomic Cl and NO_2. Atomic Cl radicals play multifaceted roles in oxidation chemistry throughout the boundary layer (Simpson et al., 2015),

including hydrocarbon oxidation (Atkinson et al., 2006a, and references therein), ozone production and destruction (Halfacre and Simpson, 2022; Liao et al., 2014; Sarwar et al., 2012, 2014; Simon et al., 2009; Wang et al., 2016), and mercury depletion (Driscoll et al., 2013). However, the quantitative magnitude to which they affect these processes remains an open question. On the other hand, NO_2 is one of the principal components of photochemical smog and the major anthropogenic precursor for ozone production. Accounting for all sources of NO_2 is therefore important for accurately informing chemical and air quality models.

The first in situ observation of ambient $ClNO_2$ was reported by Osthoff et al. (2008) utilising chemical ionization mass spectrometry (CIMS) in the polluted marine boundary layer. CIMS has since been used in a multitude of studies for additional $ClNO_2$ observations worldwide, including North America (Jaeglé et al., 2018; Lee et al., 2018a, b; Mielke et al., 2011; Riedel et al., 2012, 2013; Thornton et al., 2010; Wagner et al., 2013; Young et al., 2012), Europe (Bannan et al., 2015; Phillips et al., 2012; Sommariva et al., 2018; Tan et al., 2022), Asia (Le Breton et al., 2018; Liu et al., 2017; Tham et al., 2016, 2018; Wang et al., 2022, 2016, 2017; Xia et al., 2020; Ye et al., 2021; Yu et al., 2020; Zhou et al., 2018), in the presence of snow/ice (Kercher et al., 2009; McNamara et al., 2020), and in indoor air quality studies (Moravek et al., 2022). Limits of detection are often reported at 10^0 pptv under 25-30 s averaging times, (Bannan et al., 2015; Kercher et al., 2009; McNamara et al., 2020; Mielke et al., 2011), and has been recently reported at sub-pptv for 1 s measurements (Decker et al., 2024). Typical observed mixing ratios range from $10^1 – 10^3$ pptv, with the highest levels observed in coastal polluted regions, where sources of nitrogen oxides and Cl^--rich aerosols are plentiful (Wang et al., 2019, 2021, and references therein).

While CIMS is a highly effective technique, $ClNO_2$ quantitation involves non-trivial calibration work. A laboratory source of $ClNO_2$ may be readily generated by flowing a known amount of N_2O_5 across a Cl^--containing salt bed (or Cl_2 across NO_2^--containing salt bed), but its quantitation assumes unit conversion out of the salt bed (e.g., Osthoff et al., 2008) or requires additional equipment to observe $ClNO_2$ thermal dissociation products, such as a thermal dissociation-cavity ring down spectrometer (TR-CRDS) (Thaler et al., 2011) or a cavity attenuated phase shift spectrometer (CAPS) (e.g., Tan et al., 2022). Further, I^- based CIMS demonstrates variable sensitivities based on the temperature and relative humidity of the ion-molecule reactor, thereby requiring substantial laboratory work to develop humidity- and temperature-dependent calibration factors (Lee et al., 2014; Robinson et al., 2022). Thus, there is an opportunity to innovate a method that can detect $ClNO_2$ directly without the need for supplemental instrumentation.

The advantages of optical methods include analyte specificity and near absolute detection, utilizing well-defined physical absorption properties, and requiring only infrequent calibrations or method validation procedures. Thaler et al. (2011) previously used a TR-CRDS system to detect $ClNO_2$ as NO_2 by absorption at 405 nm under laboratory conditions, achieving CIMS-competitive metrics (e.g., reported 20 pptv limit of detection for 1 minute averaging). This was achieved by flowing sample air through both an unheated reference pathway and a heated (450 ^oC) sample pathway, under which $ClNO_2$ would thermally dissociate into Cl radicals and NO_2 (Reaction R1).

$$ClNO_2\,(g) + \text{heat} \rightarrow Cl(g) + NO_2(g) \qquad \text{(R1)}$$

The difference in observed NO_2 signal between the two channels provided a quantitative $ClNO_2$ measurement. However, its use for conducting field measurements was reported to be limited, as the thermal degradation of alkyl nitrates (i.e., PAN) into NO_2 cannot be distinguished from NO_2 originating from $ClNO_2$ due to overlapping thermal dissociation profiles.

For this same thermal-dissociation setup, product chlorine radicals will react quickly (e.g., Cl radical lifetime of 0.2 s for typical CH_4 mixing ratios of 2 ppmv and $k_{298} = 1 \times 10^{-13}$ cm^3 $molecule^{-1}$ s^{-1} (Bryukov et al., 2002)) with ambient

hydrocarbons (e.g., methane) to form hydrogen chloride (HCl), which is a stable reservoir species for reactive chlorine (Reaction R2).

$$Cl\,(g) + RH\,(g) \rightarrow HCl(g) + R(g) \quad (R2)$$

Several optical methods for the high-frequency and precise detection of HCl have recently been reported that overcome historical challenges with its sampling (Furlani et al., 2021; Hagen et al., 2014; Halfacre et al., 2023; Wilkerson et al., 2021), making them attractive candidates for an alternative thermal dissociation approach for the detection of $ClNO_2$. In this work, we demonstrate the coupling of a thermal dissociation furnace to HCl-TILDAS (TD-TILDAS) for quantitative detection of $ClNO_2$ as HCl. Compared with CIMS, TD-TILDAS is a lower time-cost method for determining $ClNO_2$ mixing ratios, involving less experimental calibration work and simpler data processing as a direct method.

2 Methods

2.1 $ClNO_2$ Generation

$ClNO_2$ was synthesized by flowing Cl_2 across a nitrite-rich slurry, as described by Thaler et al. (2011) and shown by Reaction R3.

$$Cl_2(g) + NO_2^-(aq) \leftrightarrow ClNO_2\,(g) + Cl^-(aq) \quad (R3)$$

However, it is believed the $ClNO_2$, once produced, may react further by dissolving into the water, hydrolyzing, and producing nitronium and chloride ions (R4) (Frenzel et al., 1998).

$$ClNO_2\,(g) + H_2O\,(l) \leftrightarrow Cl^-\,(aq) + NO_2^+\,(aq) \quad (R4)$$

The nitronium ion can then react with NO_2^- to produce N_2O_4, which exists in equilibrium with NO_2 (R5).

$$N_2O_4\,(g) \leftrightarrow NO_2\,(g) + NO_2\,(g) \quad (R5)$$

As detailed by Thaler et al. (2011), this chemistry can be mitigated by minimizing the residence time of $ClNO_2$ in the reaction vessel and, to a lesser extent, by increasing the Cl^- content of the slurry to encourage the equilibrium in R4 towards $ClNO_2$. Therefore, we composed our slurry using sodium chloride (>99.5% pure, BioXtra, Sigma Aldrich product no S7653-5KG, USA) and sodium nitrite (99%, extra pure, Acros Organics Code 196620010, Belgium) at a mole ratio of 100:1 Cl^-:NO_2^-, wetting with 18MΩ deionized water (Millipore). The slurry was housed in ~10 cm of 1.25 cm diameter PFA tubing. Varied flow rates (0.5-5 mL min^{-1}) of 10 ppmv Cl_2 (diluted in nitrogen, BOC product no. 150916-AV-B, United Kingdom) were injected into a dilution flow (ranging from 200-2499.5 mL min^{-1}) of NO_x-scrubbed compressed air (using trap composed of 50% Sofnofil (Molecular Products Ltd., Essex, United Kingdom) and 50% activated carbon) that was subsequently passed over the slurry, generating $ClNO_2$. A portion of the dilution flow was directed into a bubbler containing 18MΩ deionized water prior to entering the slurry to maintain a humid environment and prevent the slurry from drying out. A schematic diagram of this setup is presented in Fig. 1a.

2.2 TD-TILDAS

The TILDAS instrument and operation technique have been well-described previously (McManus et al., 2011, 2015). HCl-TILDAS was developed by Aerodyne Research, Inc. and characterized by Halfacre et al. (2023). Briefly, air is sampled at 3.0 L min^{-1} through a heated (50 °C) quartz "inertial inlet," which is a type of virtual impactor used to remove particles >300 nm from the sample matrix. Sample air continues its flow through 3 m of heated (50 °C) tubing into the Herriott cell (204 m pathlength) inside the TILDAS. HCl is then detected via a mid-IR inter-band cascade laser that probes the strong R(1) $H^{35}Cl$ absorption line at 2925.89645 cm^{-1} within the (1-0) rovibrational absorption band (Guelachvili et al., 1981).

Nitryl chloride was converted to HCl for detection by TILDAS via thermal dissociation and the subsequent reaction of Cl radicals with hydrocarbons, namely methane (Reactions R1-R2) (Thaler et al., 2011). While modelling results predicted ambient mixing ratios of methane (~2 ppmv) are sufficient for achieving unit conversion of 1 ppbv $ClNO_2$ to HCl (Sect. 3.1), the sample flow was additionally spiked with propane (BOC Limited, product no. 34-A) to a mixing ratio of 5 ppmv to both ensure reaction completeness and outcompete Cl wall losses, as the rate constant for the reaction between Cl and propane is 3 orders of magnitude faster than with methane (Atkinson et al., 2006a). Next, the sample was directed to a 90 cm length of quartz tubing (9.5 mm OD, 7.5 mm ID) housed within a furnace (Carbolite Gero TS1 12/60/450) upstream of the inertial inlet. Sixty centimetres of this tubing is held within the heated region of the furnace, resulting in a residence time of ~500 ms under a flow rate of 3 L min^{-1}. The internal temperature of the furnace is monitored using the furnace's inbuilt temperature sensors and logged using the furnace software. To mitigate HCl surface interactions after $ClNO_2$-conversion, perfluorobutane-1-sulfonic acid (PFBS; Merck, product no. 562629, United Kingdom) vapor was introduced just after the furnace to actively passivate tubing and inlet surfaces, improving HCl transmission to the TILDAS inlet by 1) displacing HCl sorbed to surfaces and 2) increasing the non-polar character of surfaces by presenting a fluorinated chain to passing analytes (Halfacre et al., 2023; Roscioli et al., 2016). As detailed by Halfacre et al. (2023), a flow (50-75 mL min^{-1}) of oxygen-free nitrogen was flowed into the headspace of a Teflon bubbler containing 5 g of PFBS, thereby flushing the PFBS vapor into the sample line. A schematic diagram of this setup is presented in Fig. 1b.

The major sources of uncertainty with using TD-TILDAS to detect $ClNO_2$ include the degree of $ClNO_2$ conversion to HCl, instrument noise, background drifts, and potential line losses of HCl. Confirmation of the unit conversion of $ClNO_2$ to HCl was confirmed by modelling and laboratory experiments (see Sects. 3.1 and 3.2). Instrument noise and background drifts were assessed regularly from blanks. For laboratory experiments, blanks were performed by sampling the $ClNO_2$ standard (Sect. 2.1) diluted in NO_x-scrubbed compressed air through the unheated furnace. This dilution air was generated using an air compressor and dehumidifying system (dew point approximately −60 °C, absolute water vapor concentration ~ 0.01%). To vary sample humidity, carrier gas flow was split such that varied amounts were passed through a bubbler containing deionized water. Concerning line losses of HCl, the only source of HCl will be from $ClNO_2$ conversion during laboratory experiments, and therefore line losses were assessed between the furnace and the inertial inlet. As detailed in Fig. 1b, 30 mL min^{-1} of flow from a homemade HCl permeation source (Furlani et al., 2021; Halfacre et al., 2023) was injected alternatingly before the furnace and just before the inertial inlet to determine loss of HCl over this region. So long as unit conversion of $ClNO_2$ to HCl can be confirmed and blank / line losses are corrected, this method will be as accurate as the TILDAS is for detecting HCl, which was previously found to be within the 5% tolerance of a commercial HCl cylinder with a certified concentration (Halfacre et al., 2023).

For ambient sampling (Fig. 1c), an additional 5m of 1.25 cm OD PTFA Teflon was added before the tee that splits the CIMS and TILDAS flow paths to sample outside air. A 5 µm PFA Teflon filter was also installed to collect particulates, reducing the potential for HCl displacement through thermodynamic partitioning of particulate Cl^- that would otherwise enter

the heated furnace (Huffman et al., 2009). This Teflon filter was not found to affect the observed mixing ratio of our $ClNO_2$ standard in measurement comparisons with and without the filter. However, the collection of particulates on the filter could enable heterogenous chemistry with passing N_2O_5 plumes that may produce corresponding $ClNO_2$ plumes that are not reflective of ambient chemistry, and so frequent replacement of these filters is necessary (e.g., daily). Blank air was generated by pumping ambient air through a 50% activated carbon / 50% Sofnofil scrubber, which was found to effectively remove $ClNO_2$ from the sample stream. The pump (KNF model N035.1.2AN.18) was able to overblow the sample inlet at a flow rate of ~25 L min^{-1}. This approach is favoured over the use of synthetic cylinder air as significant changes in sample humidity can result in release of HCl from surfaces (Halfacre et al., 2023). Blanks were performed for 10 minutes every 30 minutes to ensure the instrument had enough time to respond and adjust to a stable background value. Additionally, ambient measurements will include HCl, which would act as an interference for $ClNO_2$ observations. To obviate this, a denuder (coating of 2% Na_2CO_3 and 2% glycerol dissolved in 50% water and 50% methanol) was installed before the furnace to selectively remove acidic gases (e.g., HCl, HNO_3) that may influence quantitation. Using the denuder for this purpose was found to be effective for at least one-week periods, after which it was generally replaced to avoid coating exhaustion. The denuder was also found to affect $ClNO_2$ throughput on shorter term timescales (e.g., daily), with a freshly coated denuder causing as much as 55% loss of the $ClNO_2$ standard mixing ratio. This was determined by calculating the percent difference when sampling the $ClNO_2$ standard both through and bypassing the denuder. Because $ClNO_2$ additions during ambient sampling will always be added through the denuder, it was important that the $ClNO_2$ standard (Sect. 2.1) was sampled in dry air before and after overnight experiments to quantify how this loss evolved over the course of an experiment such that data could be corrected using the percent difference term. Periodic additions of HCl standard were also performed to assess line losses of HCl after conversion in the furnace. In contrast to the laboratory experiment configuration, permeation source HCl in blank air was only injected just downstream of the furnace mid-experiment to reduce exposure of unpassivated sampling surfaces to HCl. Losses were assessed by comparing this observed HCl injection value to pre- and post-experiment injections over dry compressed air. Injections of HCl and $ClNO_2$ standards was controlled using 3-way Teflon solenoid valves (MasterFlex Model no. 01540-18, Cole Parmer, United Kingdom).

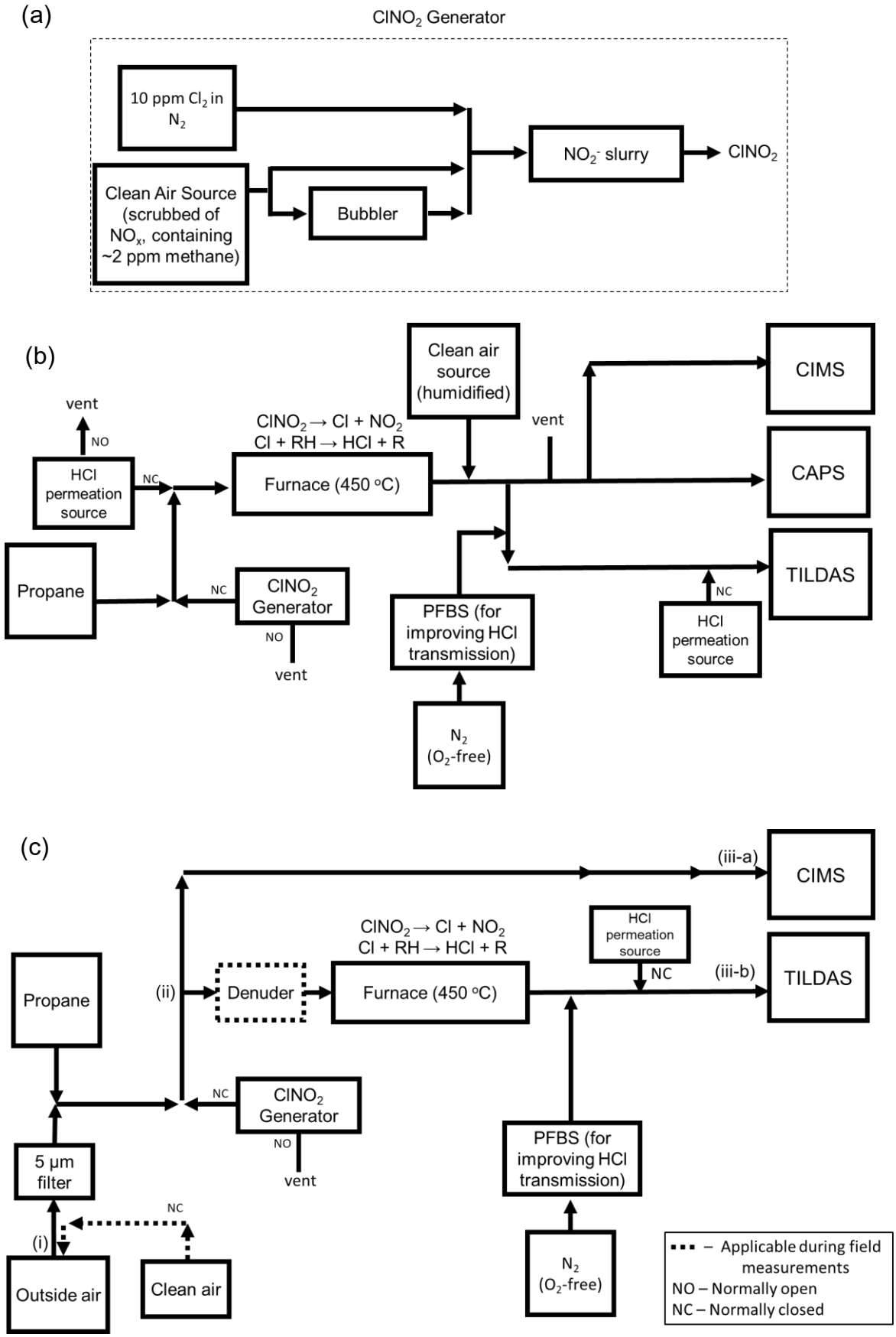

Figure 1 Experimental schematic diagrams for (a) generating $ClNO_2$, b) laboratory comparison measurements between CIMS, TILDAS, and CAPS NO_2, and (c) calibration/field sampling between CIMS and TILDAS. Note that "NO" stands for "normally open" and "NC" stands for "normally closed" in reference to solenoid valves that control the flow direction for these items. For (c), the approximate distance between point (i) and (ii) is 5 m, from (ii) to (iii-a) is 1.5 m, and from ii to (iii-b) is 2 m.

2.3 Supporting Instrumentation

To confirm the efficacy of TD-TILDAS as a valid quantitative method for $ClNO_2$ detection, testing was performed simultaneously with a Cavity Attenuated Phase Shift (CAPS) NO_2 instrument (Sect. 2.3.1) and Time of Flight-Chemical Ionization Mass Spectrometer (Sect. 2.3.2), both of which have previously reported as $ClNO_2$ detection methods.

2.3.1 Cavity Attenuated Phase Shift (CAPS) NO_2

$ClNO_2$ mixing ratios observed by the TILDAS were confirmed via simultaneous detection of the NO_2 product of $ClNO_2$ thermal dissociation using a commercial Cavity Attenuated Phase Shift NO_2 detector (Teledyne T500U CAPS). Briefly, emission from a LED (emission centred around 425 nm) is reflected across two spherical mirrors and absorbed by NO_2 in the optical cell. This difference in light is detected by a photodiode and quantified based on its absorbance via the Beer-Lambert Law. The instrument was calibrated using gas-phase titration of NO by O_3 to produce varied concentrations of NO_2. A 1ppm NO in nitrogen cylinder (certified 982 ppb, NPL) was used to verify the concentration of NO in a 25ppm NO in nitrogen working standard (BOC). A multigas blender (Environics S6100) was used to generate a range of O_3 concentrations (range 0-130 ppbv) for titrating some of the NO (NO in excess, 200 ppbv) into NO_2, and the decrease in the NO concentrations was measured using a calibrated NO_x instrument (Teledyne API Chemiluminescence T200). The NO_2 introduced to the CAPS instrument is thus the sum of the drop of NO from the added ozone and the NO_2 already present in the working standard. The T200 NO_x instrument was also used to measure ambient air alongside the CAPS (range 0-25 ppbv), and these data are presented in Fig. A1. Additionally, the Teledyne T500U includes an internal drying assembly and has a manufacturer recommended humidity range of 0 – 95%.

2.3.2 Time of Flight Chemical Ionisation Mass Spectrometry (CIMS)

$ClNO_2$ was additionally detected using a VOCUS high-resolution chemical ionization time-of-flight CIMS (Tofwerk, Switzerland) with a VOCUS AIM reactor and using iodide (I^-) as a reagent ion gas. A complete description of this instrument and its operational principles are described in detail by Riva et al. (2024). Briefly, sample gas is drawn into the sampling inlet and pulled through a critical orifice (0.475 mm) and PFA Teflon sample flow guide into a conical ion-molecule reactor (IMR) at a flow rate of 1.8 L min^{-1}. The IMR was held at a constant pressure of 50 mbar using a vacuum pump (IDP3, Agilent Technologies) and temperature controlled to 50 °C. The reagent ion source was a permeation tube containing trace amounts of CH_3I dissolved in benzene (Tofwerk). Ultra-high purity, oxygen-free N_2 gas (generated by flowing compressed air through gas with a commercial N_2 generator, Infinity NM32L, Peak Scientific Instruments, UK) is continually flowed over the permeation tube to flush the gaseous CH_3I/benzene mixture into a compact vacuum ultraviolet ion source (VUV). Within the VUV, UV light emitted from a Kr lamp (116.486 nm and 123.582 nm) is absorbed by benzene, generating low energy photoelectrons that can react with CH_3I to produce I^- (Ji et al., 2020). The I^- reacts with analytes for approximately 30 ms before being drawn through another critical orifice where the sample travels through four differentially pumped chambers before reaching the drift region of the ToF-CIMS. Ions in the ToF chamber are extracted and converted into mass spectra via an MCP detector with a preamplifier over a mass range of 7-510 Th. The extracted packets are averaged over a period of 1 second and the resolution of the instrument is ≈ 5000. Data was collected at a rate of 1 Hz. Data averaging, mass calibration, peak assignment, peak fitting and peak integration are all performed using the software package Tofware (version 4.0.0, TOFWERK) used in Igor Pro 9 software (Wavemetrics). Peak fitting focused on $I^{35}ClNO_2^-$ (m/z 207.8668) and $I^{37}ClNO_2^-$ (m/z 209.8638), and isotope abundances were manually confirmed to be ~1:0.32, based on the natural abundance of chlorine isotopes. CIMS signals were normalized against the sum of the total number of reagent ions, which is equivalent to $I^- + I(H_2O)^-$

. Additionally, as the CIMS sensitivity to $ClNO_2$ varies with humidity in the ion-molecule reactor region, we define an additional term equal to ratio of the iodide water cluster ($I(H_2O)^-$) to the reagent ion sum ($I^- + I(H_2O)^-$), hereafter referred to as the Iodide Water Ratio (IWR). Instrument backgrounds were assessed using air scrubbed of $ClNO_2$, as described in Sect. 2.2.

2.4 Data Analysis

Data analysis was conducted using the R language for statistical computing (R Core Team, 2021). Linear regressions were calculated using the York method (Cantrell, 2008) when possible so as to incorporate uncertainties in compared variables.

2.5 Chemical Modelling

The 0-D box model Kintecus (Ianni, 2003, 2022) was used to explore the gas phase chemistry occurring in the heated furnace to predict the timescales of the thermal-dissociation of $ClNO_2$ and the subsequent formation of HCl after reaction with hydrocarbons (Reaction R2). The only hydrocarbon included in these model experiments was methane. The model was also used to identify potential interferents that could prevent unit conversion of $ClNO_2$ to HCl. The results of the model were used to guide the experimental set-up. The modelled species, reaction list, tested interferents (including ClNO and alkenes), and initial concentrations are included in the Appendix (Tables A1-A3). Reaction kinetics were sourced from the NIST Chemical Kinetics Database and IUPAC Evaluated Kinetic Data websites (Manion et al., 2015; Wallington et al., 2021), and primary literature references are listed next to each reaction. No chemical species were held constant or were otherwise constrained outside of initial concentrations. The model integration time was set to 1 ms, and the entire simulation was set to last 150 ms. The model initiated with a temperature of 25 ^oC (held for 10 ms) before increasing to 450 ^oC over the course of 22 ms. The temperature was held at 450 ^oC for 40 ms, before gradually decaying back to 25 ^oC over 70 ms.

3 Results & Discussion

3.1 Modelling TD Chemistry

Box model simulations predicted the rapid, virtually unit conversion of $ClNO_2$ to HCl after increasing temperature to 450 ^oC (Fig. 2) under the model conditions outlined in Tables A1-A3. Ninety percent conversion was calculated to occur within 23 ms from a starting $ClNO_2$ concentration of 2.46×10^{10} molecules cm^{-3} (1 ppbv at 25 ^oC), and ambient mixing ratios of methane (i.e., 2 ppmv at 25^oC) were found to be sufficient for facilitating this chemistry. While Cl-mediated hydrocarbon oxidation was shown to produce a modest enhancement of hydroxyl radical concentrations (Fig. 2b), it was not enough to compete meaningfully with Cl to mitigate or retard Reaction R1. Similarly, an initial O_3 concentration of 9.84×10^{11} molecules cm^{-3} (40 ppbv at 25^oC) did not significantly inhibit the desired chemistry by the direct reaction of O_3 with Cl radicals.

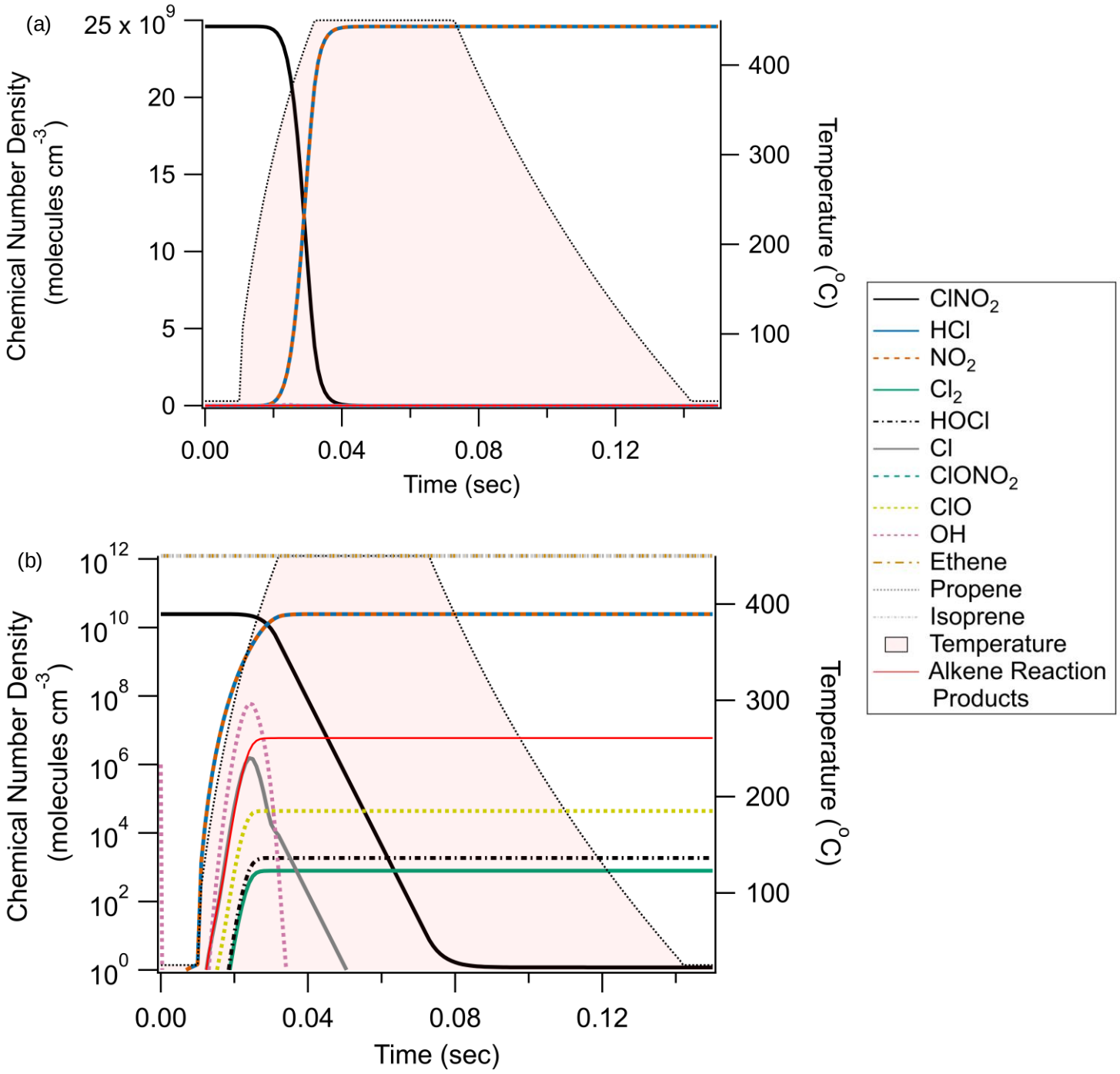

Figure 2: Chemical modelling results of the thermal dissociation of $ClNO_2$ and its subsequent conversion to HCl. Panel A presents results on a linear y-axis, while Panel B features the same data on a logarithmic y-axis. Note that ethene, propene, and isoprene are off-scale in Panel A (1.23 x 10^{12} molecules cm^{-3} / ~50 ppbv) to better display the relationships between $ClNO_2$, HCl, and NO_2, and are shown to remain constant in Panel B.

Concerning potential interferents, Cl can add to double bonds found on alkenes without producing HCl. Reactions with ethene, propene, and isoprene were included in the model at 1.23 x 10^{12} molecules cm^{-3} (50 ppbv at 25° C) each and were found to produce approximately 1 x 10^6 molecules cm^{-3} of non-HCl product, which is 4 orders of magnitude less than the HCl converted from $ClNO_2$. As these mixing ratios of alkenes are larger than those typically found in real world environments (e.g.,

Budisulistiorini et al., 2015; Hellén et al., 2024; Tripathi et al., 2021), it is therefore unlikely alkenes will cause meaningful interference for $ClNO_2$ quantification.

$ClNO_2$ was predicted to be the only known inorganic chlorine reservoir to thermally dissociate at 450 °C. This is consistent with the relative bond dissociation energies found for $ClNO_2$ (142 kJ mol^{-1}) relative to the various other forms of inorganic chlorine simulated (Cl-NO_2 < Cl-Cl < Cl-O < Cl-R < Cl-H) (Darwent, 1970). Production of other inorganic chlorine compounds (e.g., Cl_2, HOCl, $ClONO_2$, or reformation of $ClNO_2$) was orders of magnitude less than the resulting HCl and is therefore not believed to influence HCl production. Even so, there remain potential inorganic chlorine species that may still act as interferents in this method. Nitrosyl chloride (ClNO) has been previously predicted by modelling to exist at ppbv-level mixing ratios in polluted marine environments and could be an efficient Cl-atom source (Raff et al., 2009). Indeed, 1 ppbv (2.46 x 10^{10} molecules cm^{-3}) of ClNO was found to partially thermally dissociate in our Kintecus model (bond dissociation energy of 159 kJ mol^{-1}) and generate additional HCl, as well as NO that was gradually converted to NO_2 (Fig. A2). On the addition of heat, ClNO decreased by 40% while HCl increased by an equivalent amount (in addition to the 2.46 x 10^{10} molecules cm^{-3} generated by $ClNO_2$ thermal dissociation). While we are unaware of any field measurements that have confirmed the presence of ClNO in the boundary layer to date, it appears likely this method would be sensitive to interference from ClNO if/where its presence is confirmed.

.Additionally, one notable class of compounds that could not be simulated were chloramines, which have recently received increased attention as relevant daytime sources of Cl atoms (A. Angelucci et al., 2023; Wang et al., 2023). Their largest known anthropogenic sources include water disinfection processes, swimming pools, and cleaning products. Trichloramine, dichloramine, and monochloramine have reported bond dissociation energies of 381, 280, 251 kJ mol^{-1}, respectively (Darwent, 1970) ($ClNO_2$ bond dissociation energy = 142 kJ mol^{-1}), and so would not be expected to produce free Cl radicals in the temperature range simulated herein if its thermochemistry is consistent with the above bond dissociation energy trend. However, to the authors' knowledge no information is available regarding their thermal stability in the gas phase at atmospherically relevant conditions, and this potential source of positive interference for our proposed method cannot be discounted via the model at this time. Similarly, prevalent organochlorides, such as methyl chloride (CH_3Cl), dichloromethane (CH_2Cl_2), chloroform ($CHCl_3$), and carbon tetrachloride (CCl_4) could cause positive interference if they dissociate and produce Cl atoms in the furnace (World Meteorological Organization, 2022). Global average mixing ratios for CH_3Cl, CH_2Cl_2, $CHCl_3$, and CCl_4 were ~ 550 pptv, ~40 pptv, 9 pptv, and 77 pptv, respectively, during 2020. Appropriate thermal dissociation kinetic parameters could not be sourced for the conditions used herein (i.e, temperatures ≤ 450 °C), and so these compounds could not be properly simulated by the Kintecus model. Similarly to the chloramines, the bond dissociation energies are much higher than other compounds simulated (339, 310, 346, 293 kJ mol^{-1} for CH_3Cl, CH_2Cl_2, $CHCl_3$, and CCl_4, respectively (Darwent, 1970; Weissman and Benson, 1983)).

3.2 Laboratory Characterization of TD-TILDAS

For laboratory characterization, a stable source of $ClNO_2$ was generated (Sect. 2.1) for assessing TD-TILDAS performance in comparison with other established $ClNO_2$ sampling techniques, including CAPS NO_2 and CIMS (Sect. 2.3). One key change between model simulations and this experimental setup is the inclusion of propane to the sample stream (estimated mixing ratio of 5 ppmv within the heated section of sample configuration). While the model predicted the pertinent chemistry will occur in ~23 ms using only ambient methane as the hydrocarbon (Sect. 3.1) and the residence time in the heated furnace is ~500 ms, adding propane ensures complete conversion of $ClNO_2$ to HCl and ensures wall losses are negligible, as Cl radicals react with propane approximately 3 orders of magnitude faster than with methane (Atkinson et al., 2006a). The fact

that no additional HCl signal was observed on addition of propane at varying levels (not shown) supports our calculations that unit conversion is achieved and competitive loss of Cl radicals to walls is negligible.

A schematic diagram of these experiments is shown in Fig. 1a. Figure 3 represents a typical comparison experiment in which $ClNO_2$ was sampled by all three instruments simultaneously. First, $ClNO_2$ was introduced into the flow stream with the furnace unheated, yielding a positive CIMS signal for $IClNO_2^-$ (~1100 ncps for the example in Fig. 3), while TILDAS HCl and CAPS NO_2 mixing ratios remained at background levels. As the furnace temperature approached 450 °C, Reactions R1-R2 began to occur. HCl and NO_2 mixing ratios rose, plateauing at similar values (~2.2 ppbv in Fig. 3) while $IClNO_2^-$ decreased to the instrument baseline, implying both Reactions R1-R2 proceeded to completion. Signals returned to their original positions once the furnace was allowed to cool back to room temperature (e.g., from 16:45 in Fig. 3). Note that HCl signal spike during the furnace's temperature ramp was seen consistently across experiments, and was most likely caused by a shift in HCl molecule partitioning between the surface of the quartz tubing toward the gas phase (Halfacre et al., 2023). Allan-Werle deviation calculations demonstrate favourable performance metrics for TILDAS while sampling $ClNO_2$, with 1 Hz precision of 11.8 pptv, and as good as 1.2 pptv with an integration time of 96 seconds (Fig. 4).

A summary of comparison experiments across varied humidities is presented in Fig. 5. The changes in HCl as observed by TILDAS correlated strongly with the changes in NO_2 observed by the CAPS instrument (Pearson correlation coefficients of 0.999, 0.997, and 0.987 for relative humidities of 11%, 44%, and 66%, respectively). However, the slopes were consistently less than unity (0.95 ± 0.01, 0.93 ± 0.02, and 0.91 ± 0.02 at 11%, 44%, and 66%, respectively), indicating observed HCl mixing ratios were less than corresponding NO_2 mixing ratios. One potential explanation for this could be loss of Cl radicals in the furnace, but we do not believe this to be the case (as detailed above). While physical losses of HCl to sampling lines would not be unexpected as HCl has a high affinity for sorbing to physical surfaces, experiments were designed to minimize these interactions, and line loss experiments were performed to quantify any losses observed at tested humidities. Experimentally, a small flow (50-75 mL min^{-1}) of PFBS vapour was injected into the TILDAS sampling line downstream of the furnace to reduce HCl affinity for surfaces (Sect. 2.2) (Note that PFBS was not introduced to the entirety of the flow path to avoid sampling of PFBS by other instruments. Additionally, there is evidence that PFBS degrades at temperatures above 400°C (Xiao et al., 2020), and so its ultimately efficacy and reproducibility within the furnace system would be uncertain). Further, the high operating temperature of the furnace would also be expected to minimize HCl-wall interactions within the quartz tubing. Indeed, no lines losses were found at 11% relative humidity between when the HCl permeation source standard was injected into the sampling line before the heated furnace (2.95 ± 0.02 ppbv) and when HCl was injected just before the inertial inlet (accounting for dilution factors) (2.95 ± 0.02 ppbv), consistent with Halfacre et al. (2023). Similar results were found at 44% relative humidity (pre-furnace value of 2.68 ± 0.03 ppbv vs 2.66 ± 0.03 ppbv when HCl was introduced at inlet), and real HCl loss was quantified at 66% relative humidity (pre-furnace value of 1.87 ± 0.03 ppbv vs 1.97 ± 0.03 ppbv when HCl introduced at inlet). Having accounted for these line losses, ANOVA calculations found no significant differences between these three slopes as presented in Fig. 3 ($F(2,19) = 0.10$, $p = 0.902$), indicating consistent performance between TILDAS and CAPS for detecting $ClNO_2$. However, it does not appear to explain the deviation from unity, which will be discussed below.

As discussed in Sect. 2.1, chemistry may occur within the slurry to produce N_2O_4, which can easily degrade at room temperature to produce two NO_2 molecules. If the N_2O_4 output from the NO_2^-/Cl^- slurry is constant over the timescale of an experiment (< 1 hr), it would be expected this additional NO_2 is readily accounted for during blank subtraction calculations. While we believe this is largely true for the experiments presented above, discrepancies in $ClNO_2$ signals were observed as the slurry aged (> ~3 weeks), with CAPS-observed NO_2 mixing ratios growing in significant excess of TILDAS-observed HCl mixing ratios (Fig. A3). Separate applications of TILDAS- and CAPS-based calibration factors (using data from Fig. 5) to concurrent CIMS $ClNO_2$ observations show closer resemblance to the TILDAS-observed mixing ratios (Fig. A3), suggesting

additional chemistry may be occurring within the salt bed that produces stable reservoirs of NO_2 that thermally dissociate in the furnace to produce undesired NO_2. This NO_2 artefact serves as a likely explanation for the sub-unity slopes presented in Fig. 5, as it would positively bias the CAPS measurements but not the TILDAS, which is only sensitive to HCl. Thaler et al. (2011) present in great detail strategies for minimizing N_2O_4 production in their study by minimizing the residence time in their $ClNO_2$ generator (0.3 s herein) and adjusting the molar ratio of Cl^-:NO_2^- of their salt bed (100:1 herein), but were ultimately unable to completely eliminate it; while we found these strategies helpful for reducing the overall NO_2 background as measured by CAPS, we found they were unsuccessful in eliminating the artefact when sample gas was passed through the heated furnace. We are not aware of such chemistry being addressed in the literature for this $ClNO_2$ generation method and do not propose potential reactions as it is outside the scope of this paper.

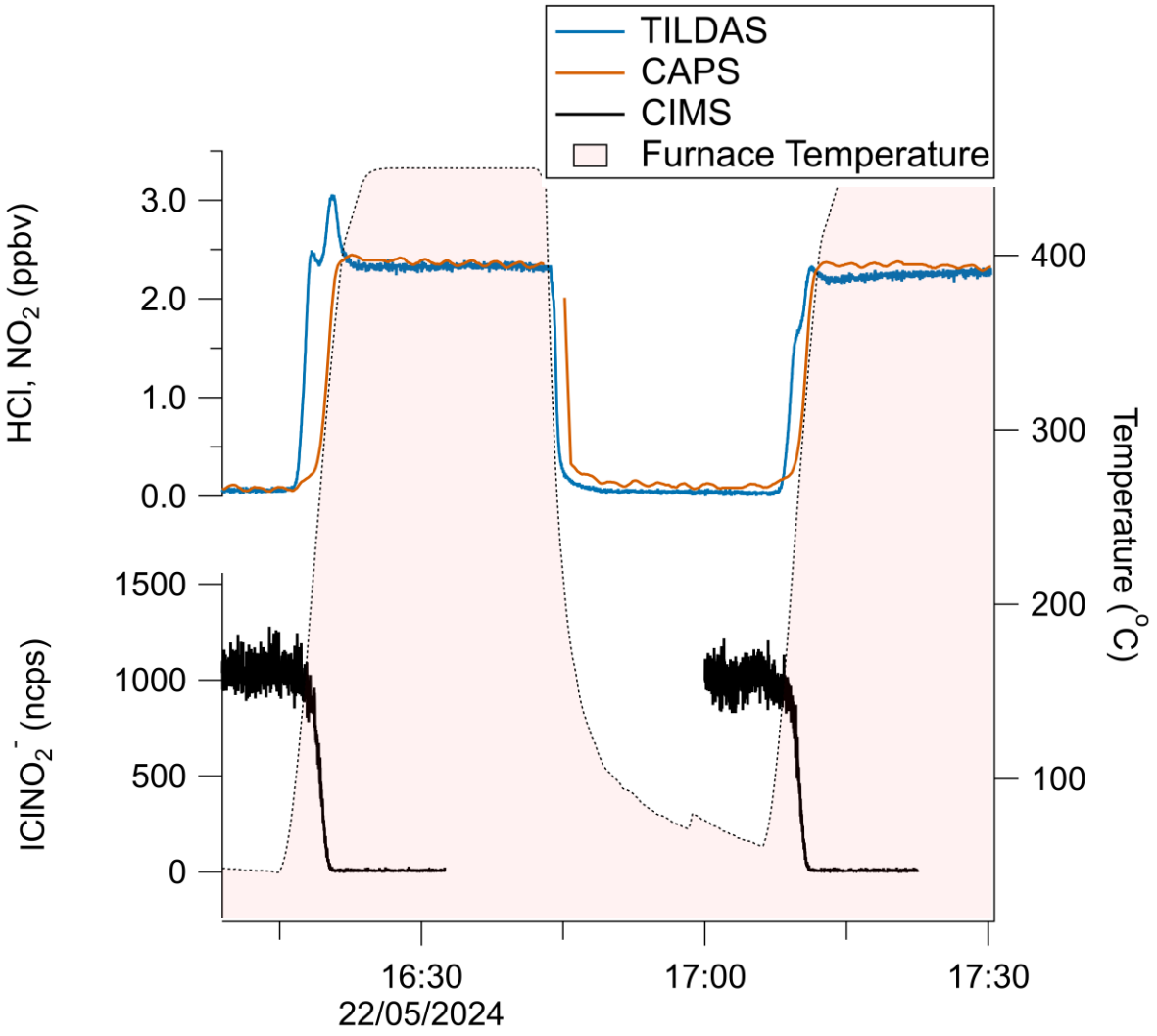

Figure 3: a) Time series demonstrating the reversible thermal conversion of $ClNO_2$ to NO_2 (red trace, CAPS) and HCl (blue trace, TILDAS), as evidenced by changes in CIMS-observed $ICl(NO_2)^-$ (black). Gaps in CIMS data are from internal CIMS tests not pertinent to this work.

Both HCl and NO_2 mixing ratios independently correlated strongly with the CIMS measurement of $ICl(NO_2)^-$ (Fig. 5b, c), and the I^- CIMS sensitivity for $ICl(NO_2)^-$ was found to vary strongly with humidity, as previously reported (Kercher et al., 2009; Mielke et al., 2011). The weakest Pearson correlation coefficient was for NO_2 and $ICl(NO_2)^-$ at 66% relative humidity ($r = 0.988$), virtually matching that of NO_2^- and HCl at the same humidity. Due to the uncertainty / unreliability of the NO_2 as it relates to $ClNO_2$ quantitation, we do not further consider the relationship between CAPS and CIMS.

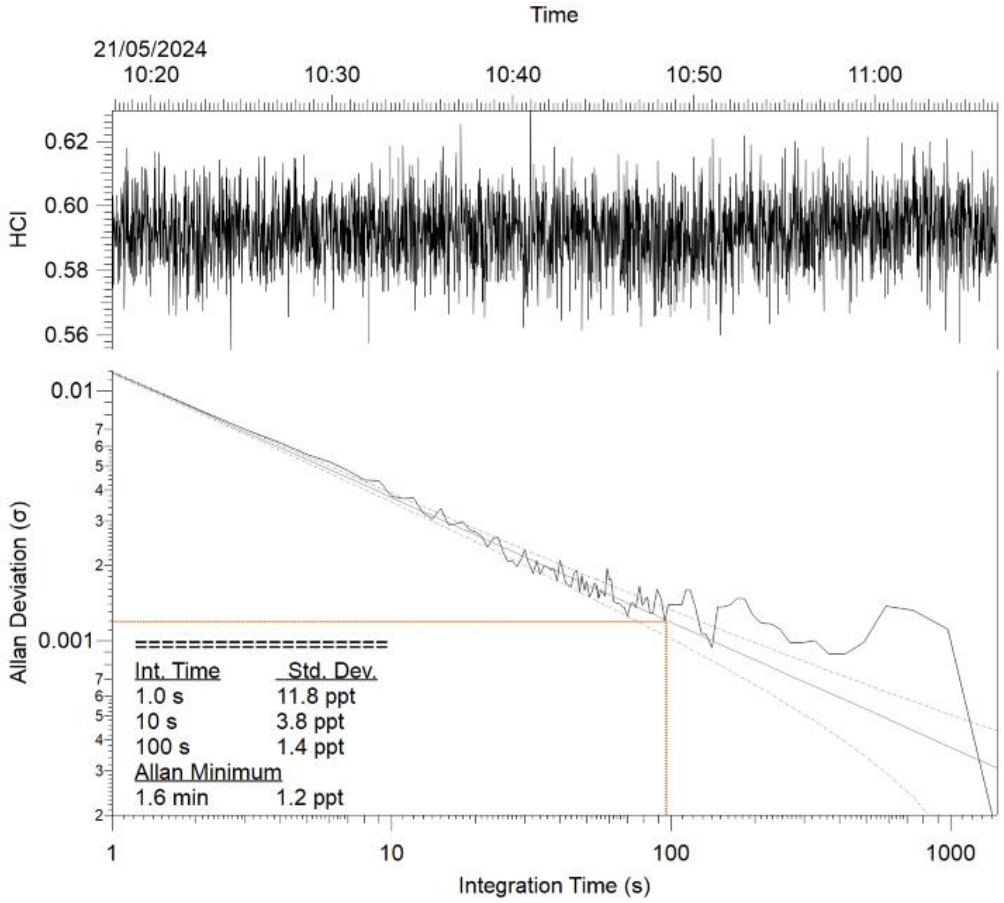

355

Figure 4: Allan-Werle plot for TD-TILDAS during addition of $ClNO_2$ standard into the sample line. The Allan minimum is indicated by the dotted red lines.

356

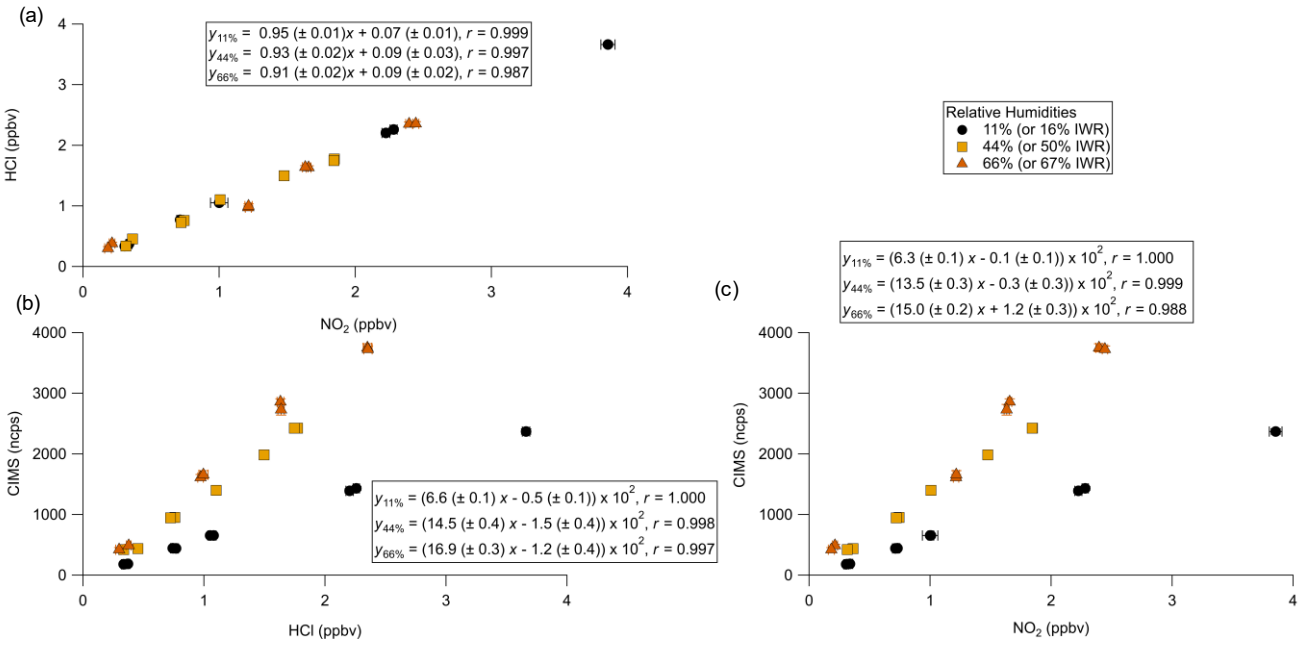

357

Figure 5 – Comparison curves of a) TILDAS vs CAPS, b) CIMS vs TILDAS, and c) CIMS vs CAPS for injections of varied mixing ratios of $ClNO_2$ across different relative humidities. Regressions involving TILDAS data have been corrected for line losses observed at 66% relative humidity.

The linear equations from Fig. 5a present significant intercepts that suggest a source of positive error for the TILDAS, and the similarity of these intercepts suggest a relatively constant/consistent source (values are statistically the same $F(4,19) = 0.624$, $p = 0.546$ per ANOVA). For these experiments, TILDAS blanks were obtained by sampling slurry air flowed through an unheated furnace; in this scenario, Reactions R1-R2 are unable to occur, and therefore any signal observed by TILDAS could be considered background. It is possible that a small amount of HCl forms in the slurry system from the aqueous disproportion reaction between Cl_2 and H_2O. When the furnace is unheated, some amount of HCl interaction with the quartz tubing is expected given there is no PFBS flow through this portion of the plumbing, biasing this blank measurement low. Then, once the furnace is heated to 450 °C, this HCl will be liberated from the quartz tubing, possibly then biasing the heated measurement high. This is supported by the presence of a peak in observed HCl as the furnace reheats (e.g., as in the second temperature ramp in Fig. 3), as some of the HCl sorbed to the furnace tube walls under room temperature is forced into the gas phase. The statistical similarity in intercepts implies this effect is constant across these experiments, leading to a consistent offset. While an ideal blank would sample the gas downstream of the slurry while selectively scrubbing $ClNO_2$, this was not practical to achieve without simultaneously scrubbing HCl. Therefore, we propose the y-intercept in these cases is a good estimate of the systematic error present in these comparison experiments.

3.3 Applicability as Field Instrument

The applicability of TD-TILDAS as a field method for $ClNO_2$ detection was tested by sampling ambient air from outside the Wolfson Atmospheric Chemistry Laboratory building on the University of York campus (York, United Kingdom) from the morning of 13 January 2025 (Fig. 6). Compared with the laboratory-based configuration described in Sect. 3.2, ambient air will contain varied amounts of HCl that would interfere with accurate quantification of $ClNO_2$ via the TILDAS method. To address this, a base-coated denuder (Sect. 2.2) was installed in the HCl sampling line. $ClNO_2$ throughput was found to be hindered when flowed through the denuder but increased over the course of the observation period (pre-experiment estimation of 55% loss on 10 January vs 31% measured directly after the experiment on 13 January). This loss was accounted for by applying a time-varying, linearly interpolated correction factor for the denuder. In addition, line losses affecting HCl between the heated furnace and TILDAS inlet were estimated as 2.7%, which was added back into the TILDAS measurements. CIMS observations of $IClNO_2^-$ were calibrated against TD-TILDAS using a mid-experiment $ClNO_2$ addition, yielding a sensitivity factor of 1982 ncps ppb^{-1} (measured with a corresponding IWR of 42%). We note that this factor is ~35% greater than the value of 1450 ncps $ppbv^{-1}$ as presented in Fig. 5b for a comparable IWR (44%); this is likely due to the replacement of the reagent ion permeation source, repair of reagent ion source heaters, and change in the overall sampling configuration between the experiments from Sect. 3.2 and this section (as illustrated by Fig. 1). Application of this sensitivity factor across this measurement period can be justified as the IWR was found to be stable (38 ± 2%). Limits of detection, based on instrument blanks, were found to average 10 ± 5 pptv for TD-TILDAS and 1 ± 1 pptv for CIMS (using 60 second data averaging).

As seen in Fig. 6a, TILDAS- and CIMS-observed $ClNO_2$ demonstrate very good agreement for these ambient observations in both signal magnitude and structure. This is quantitatively supported by regression calculations during this period that yield a slope of 0.97 ± 0.01 (Fig. 6b), which is well within the averaged combined uncertainty for this period of 9%. While the sub-unity slope could indicate small losses on the TILDAS method, pre- and post-experimental losses were tested and corrected for as detailed above, and so this is not believed to be a large source of error in this case. It is otherwise not unexpected that this slope is found to deviate from unity given the uncertainty in the application of a single-point CIMS

sensitivity factor. Nevertheless, this agreement gives us confidence that it is appropriate for these measurements and provides proof-of-concept for this TILDAS method.

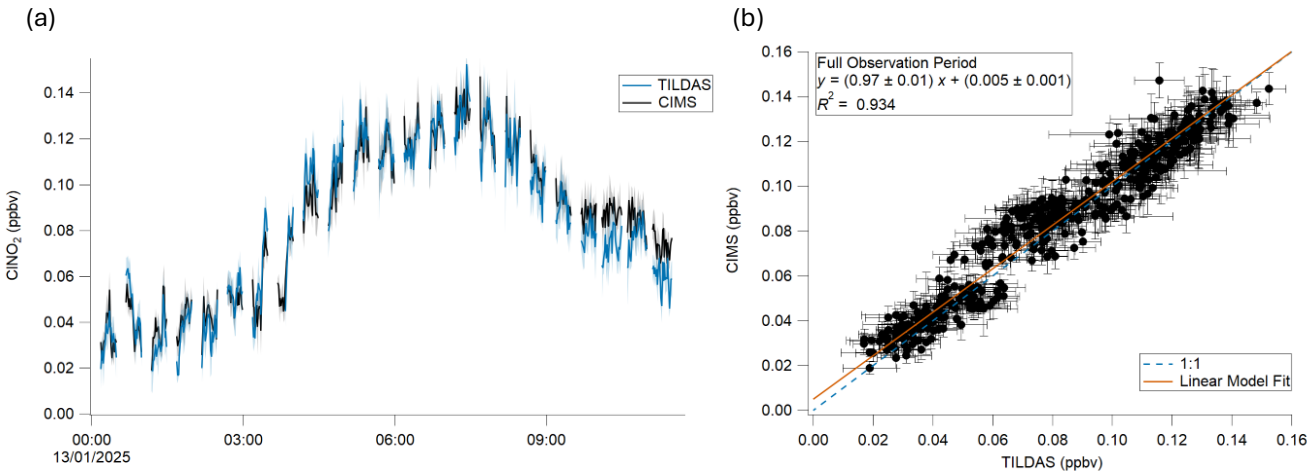

Figure 6 – a) Time series comparison of TILDAS and CIMS observations of $ClNO_2$. b) Scatter plot of data shown in panel (a). The error shading in (a) and bars in (b) represent the standard deviation of the 60 s averaged measurements.

Additional sources of measurement uncertainty include unaccounted-for thermolabile chlorine reservoirs that could cause positive interference in the TILDAS-method. As stated above, the TD-TILDAS method functions on the assumption that $ClNO_2$ is the only major chlorine source that thermally dissociates at 450 °C. As shown by the model, ClNO may be a potential source of interference if present (Fig. A2), while relevant thermochemistry information was unavailable for organochlorides and chloramines, which therefore cannot be ruled out as possible interferences by modelling. Indeed, while CIMS signals of ClNO and chloramines did not rise above their baselines during the period shown in Fig. 6, a separate measurement period demonstrates multiple occurrences where signal increases in iodide-tri- and di-chloramine adducts ($INCl_3^-$, $INHCl_2^-$) correspond with TILDAS-observed signal increases (Fig. A4). This is most dramatic at ~08:15, where ~115 ncps of $INCl_3^-$ and 18 ncps of $IHNCl_2^-$ corresponds with an increase of 100 pptv in the TILDAS signal. While these chloramine observations cannot be quantified at this time, trichloramine and dichloramine has previously been detected in downtown Toronto at ≤ 0.104 ppb and ≤ 8 ppbv, respectively (Wang et al., 2023), suggesting a combined 100 pptv interference contribution from these compounds is realistic. Synthesis and calibration of chloramine standards is a non-trivial task (Wang et al., 2023), and so further experiments are required to investigate 1) to what extent the chloramine signals can be quantified by TILDAS and 2) if the chloramine signal can be dissected from the $ClNO_2$ signal through temperature scans. The results of such experiments may therefore allow this method to be extended for the quantification of both chloramines and $ClNO_2$.

While organochlorides (e.g., CH_3Cl, CH_2Cl_2, $CHCl_3$, and CCl_4) were not explicitly measured during the period in Fig. 6, it would be expected that their potential interference in the TILDAS signal (if they dissociate in the furnace) would present as a slow varying background signal that appears as an offset above a blank, given the ubiquity of these compounds and relatively long tropospheric lifetimes for CH_3Cl, CH_2Cl_2, $CHCl_3$, and CCl_4 of 1 year, 6 months, 6 months, and 124 years, respectively (World Meteorological Organization, 2022). Such an offset, if present, could be quantified during daytime measurements (ie, when no $ClNO_2$ will be present in the boundary layer) and readily subtracted from nighttime measurements if necessary. However, the agreement between TILDAS and CIMS measurements as presented in Fig. 6 suggests this interference is not present, providing some evidence that these organochlorides are not dissociating in the furnace.

Conclusions

This work demonstrates the viability of TD-TILDAS as an independent $ClNO_2$ detection method at performance metrics comparable to quadrupole CIMS, which are more than adequate for commonly observed mixing ratios in the boundary layer. While modern CIMS instruments can achieve lower limits of detection and higher precision, the major advantage of TD-TILDAS over CIMS is that it does not require external $ClNO_2$ calibration experiments, as this work demonstrates the unity conversion of $ClNO_2$ to HCl that is subsequently detected based on well-understood spectroscopic principles. The TD method described here can thus be used effectively in laboratory settings to measure $ClNO_2$ in related experiments, or even to calibrate CIMS for $ClNO_2$ directly without needing to make assumptions regarding Cl_2 conversion on salt slurries. Additionally, use of a denuder allows this method to be readily applied to other HCl optical instruments, such as those based on CRDS.

As a field method, TD-TILDAS demonstrated excellent agreement with a co-located CIMS for $ClNO_2$ detection. The method is reliant on accurate and regular characterization of $ClNO_2$ throughput through the denuder, which was found to increase across four days of sampling. Longer-term measurement campaigns would benefit from at least weekly denuder replacements to ensure acidic gases are consistently scrubbed and do not interfere with $ClNO_2$ observations. However, the TD-TILDAS method appears susceptible to positive interference, potentially resulting from chloramines, or other unaccounted-for thermolysable chlorine compounds. Care should thus be taken should this method be deployed where large amounts of chloramines are known to be present, such as swimming pools or near water treatment facilities. More work is still required to confirm and quantify the response of this method to chloramine and organochlorides, and if so, identify an appropriate method to mitigate this potential interference. While modelling additionally suggests ClNO as an interferent, its presence in the boundary layer is yet to be confirmed through in situ observations. In any case, careful temperature ramps (e.g., Day et al., 2002) performed with the furnace in environments where unknown interferences may be a concern would likely reveal the purity of the $ClNO_2$ signal observed. Experimental adjustments could be further made for the TILDAS to alternate its sampling between a heated channel (as described in this paper) for $ClNO_2$ detection and an unheated pathway that allows for the additional detection of HCl. Doing so would require careful characterization of physical HCl losses inherent to both sampling pathways, as well as consideration of the likely hysteresis in detected HCl mixing ratios resulting from changes to the sampled air temperature that would affect the partitioning of HCl between surfaces and the gas phase.

Appendix A

Table A1 – Bimolecular reactions and parameters used for the modelling described in Sect. 2.5. Reactions follow the rate expression $k(T) = A\,(T/298)^n\,e^{-Ea/RT}$ (Burkholder et al., 2015)

Reaction	A	n	Ea (kJ mol^{-1})	Reference
$ClNO_2 + M ==> Cl + NO_2$	9.13×10^{-10}	0	106	(Baulch et al., 1981)
$Cl + Cl ==> Cl_2$	6.15×10^{-34}	0	-7.53	(Baulch et al., 1981)
$M + ClONO_2 ==> NO_2 + ClO$	2.76×10^{-5}	0	94.78	(Anderson and Fahey, 1990)
$CH_4 + Cl ==> CH_3 + HCl$	8.24×10^{-13}	2.49	5.06	(Bryukov et al., 2002)
$HCl + OH ==> H_2O + Cl$	3.74×10^{-12}	0	4.27	(Baulch et al., 1981)
$HCl + M ==> H + Cl$	7.31×10^{-11}	0	342	(Baulch et al., 1981)
$CH_3 + HCl ==> CH_4 + Cl$	3.89×10^{-13}	0	9.64	(Baulch et al., 1981)
$CH_3 + NO_2 ==> CH_3O + NO$	3.44×10^{-11}	0	0	(Srinivasan et al., 2005)
$O_3 + M ==> O + O_2$	7.6×10^{-10}	0	93.12	(Heimerl and Coffee, 1979)
$CH_3 + O ==> CH_2O + H$	2.26×10^{-11}	0	0	(Baulch et al., 1992)
$HCl + O ==> OH + Cl$	7.07×10^{-14}	2.87	14.72	(Mahmud et al., 1990)
$OH + CH_4 ==> CH_3 + H_2O$	4.16×10^{-13}	2.18	10.24	(Srinivasan et al., 2005)
$Cl_2 + M ==> Cl + Cl$	3.85×10^{-11}	0	196	(Baulch et al., 1981)
$Cl + Cl ==> Cl_2$	6.15×10^{-34}	0	-7.53	(Baulch et al., 1981)
$Cl_2 + O ==> ClO + Cl$	4.17×10^{-12}	0	11.39	(Baulch et al., 1981)
$Cl_2 + H ==> HCl + Cl$	1.43×10^{-10}	0	4.91	(Baulch et al., 1981)
$Cl_2 + OH ==> HOCl + Cl$	3.60×10^{-12}	0	9.98	(Atkinson et al., 2007)
$CH_3 + O_2 ==> CH_3O + O$	2.19×10^{-10}	0	131	(Baulch et al., 1992)
$ClO + O ==> O_2 + Cl$	2.50×10^{-11}	0	-0.91	(Atkinson et al., 2007)
$OH + ClO ==> HO_2 + Cl$	6.86×10^{-12}	0	-2.49	(Atkinson et al., 2007)
$OH + ClO ==> HCl + O2$	4.38×10^{-13}	0	-2.49	(Atkinson et al., 2007)

$CH_3O + NO ==> CH_2O + HNO$	4.00×10^{-12}	-0.7	0	(Atkinson et al., 1992)
$CH_3O + O_2 ==> CH_2O + HO_2$	7.20×10^{-14}	0	8.98	(Atkinson et al., 1992)
$HOCl + O ==> OH + ClO$	1.70×10^{-13}	0	0	(Atkinson et al., 2007)
$ClCO + M ==> CO + Cl$	4.10×10^{-10}	0	24.6	(Atkinson et al., 2007)
$O_3 + NO ==> O_2 + NO_2$	1.40×10^{-12}	0	10.9	(Atkinson et al., 2004)
$CH_3O_2 + NO ==> CH_3O + NO_2$	2.30×10^{-12}	0	-2.99	(Atkinson et al., 2006b)
$HO2 + NO ==> NO_2 + OH$	3.6×10^{-12}	0	-2.24	(Atkinson et al., 2004)
$CH_2O + Cl ==> HCl + HCO$	8.20×10^{-11}	0	0.28	(Atkinson et al., 1992)
$CH_2O + OH ==> HCO + H_2O$	4.73×10^{-12}	1.18	-1.87	(Baulch et al., 1992)
$CH_3O_2 + HO_2 ==> CH_3OOH + O_2$	3.80×10^{-13}	0	-6.49	(Atkinson et al., 1992)
$CH_3OOH ==> CH_3O + OH$	6.00×10^{14}	0	177	(Baulch et al., 1994)
$HCO + O_2 ==> CO + HO_2$	5.20×10^{-12}	0	0	(Atkinson et al., 2006b)
$CO + OH ==> CO_2 + H$	5.40×10^{-14}	1.5	-2.08	(Baulch et al., 1992)
$Cl + HO_2 ==> HCl + O_2$	1.80×10^{-11}	0	-1.41	(Atkinson et al., 1992)
$Cl + HO_2 ==> ClO + OH$	6.30×10^{-11}	0	4.74	(Atkinson et al., 2007)
$Cl + O_3 ==> ClO + O_2$	2.80×10^{-11}	0	2.08	(Atkinson et al., 2007)
$CO + Cl ==> ClCO$	1.33×10^{-33}	-3.8	0.00	(Atkinson et al., 2007)
$OH + HOCl ==> H_2O + ClO$	5.00×10^{-13}	0	0	(Atkinson et al., 2007)
$ClO + HO_2 ==> HOCl + O_2$	2.20×10^{-12}	0	-2.8	(Atkinson et al., 2007)
$ClO + ClO ==> Cl_2 + O_2$	1.00×10^{-12}	0	13.22	(Atkinson et al., 2007)
$ClO + ClO ==> OClO + Cl$	3.50×10^{-13}	0	11.39	(Atkinson et al., 2007)
$ClO + ClO ==> ClOO + Cl$	3.00×10^{-11}	0	20.37	(Atkinson et al., 2007)
$ClO + NO ==> Cl + NO_2$	6.20×10^{-12}	0	-2.45	(Atkinson et al., 2007)
$CH_2O + O ==> HCO + OH$	1.78×10^{-11}	0.57	11.56	(Baulch et al., 1992)

$OH + NO_2 ==> HNO_3$	2.70×10^{-11}	0	0	(Troe, 2012)
$CH_3Cl + OH ==> CH_2Cl + H_2O$	1.40E-12	1.6	8.65	(Cohen and Westberg, 1991)
$CH_3Cl + H ==> CH_3 + HCl$	6.14E-11	0	38.9	(Westenberg and deHaas, 1975)
$CH_3Cl + CH_3 ==> CH_4 + CH_2Cl$	2.09E-12	0	48.6	(Macken and Sidebottom, 1979)
$CH_3Cl + Cl ==> CH_2Cl + HCl$	3.30E-11	0	10.39	(Atkinson et al., 2008)
$CHCl_3 + Cl ==> CCl_3 + HCl$	4.90E-12	0	10.31	(Atkinson et al., 2008)
$Cl + C_3H_6 ==>$ Products	2.70E-10	0	0	(Atkinson et al., 2006b)
$Cl + C_5H_8 ==>$ Products	4.30E-10	0	0	(Orlando et al., 2003)
$ClNO + M ==> Cl + NO$	2.16E-09	0	134	(Baulch et al., 1981)

457

458

Table A2 – Termolecular reactions and parameters used for the modelling described in Sect. 2.5. The effective rate constant is calculated by combing the low- and high-pressure limit expressions into the following formula: $k_f(T,[M]) = \left\{\frac{k_\infty(T)k_0(T)[M]}{k_\infty(T)+k_0(T)[M]}\right\} 0.6^{\{1+[log_{10}(\frac{k_0(T)[M]}{k_\infty(T)})]^2\}^{-1}}$

Reaction	Low-Pressure Limit $k_0 = k_0^{298}(T/298)^{-n}$		High Pressure Limit $k_\infty = k_\infty^{298}(T/298)^{-n}$		Reference
	k_0^{298}	n	k_∞^{298}	m	
Cl + NO_2 + M ==> $ClNO_2$ + M	1.8×10^{-31}	2	1.1×10^{-10}	1	(Burkholder et al., 2015)
CH_3 + O_2 + M ==> CH_3O_2 + M	4.1×10^{-31}	3.6	1.2×10^{-12}	-1.1	(Burkholder et al., 2015)
Cl + C_2H_4 + M ==> Products	1.6×10^{-29}	3.3	3.1×10^{-10}	1	(Burkholder et al., 2015)

Table A3 – Initial concentrations for specified species simulated in model, and listed mixing ratios are based on a temperature of 20 °C. Potential interferents were tested in separate model runs according to the groupings on each line below, and were otherwise initiated with a concentration of 0 molecules cm^{-3}. All other compounds were initialised with a concentration of 0 molecules cm^{-3}.

Species	Initial Concentration (molecules cm^{-3})
$ClNO_2$	2.46×10^{10} (1 ppbv)
N_2	1.92×10^{19} (78%)
O_2	5.17×10^{19} (21%)
CH_4	4.92×10^{13} (2000 ppbv)
OH	1×10^{6}
O_3	9.84×10^{11} (40 ppbv)
Potential Interferents	
ClNO	2.46×10^{10} (1 ppbv)
Ethene, Propene, Isoprene	1.23×10^{12} (50 ppbv)

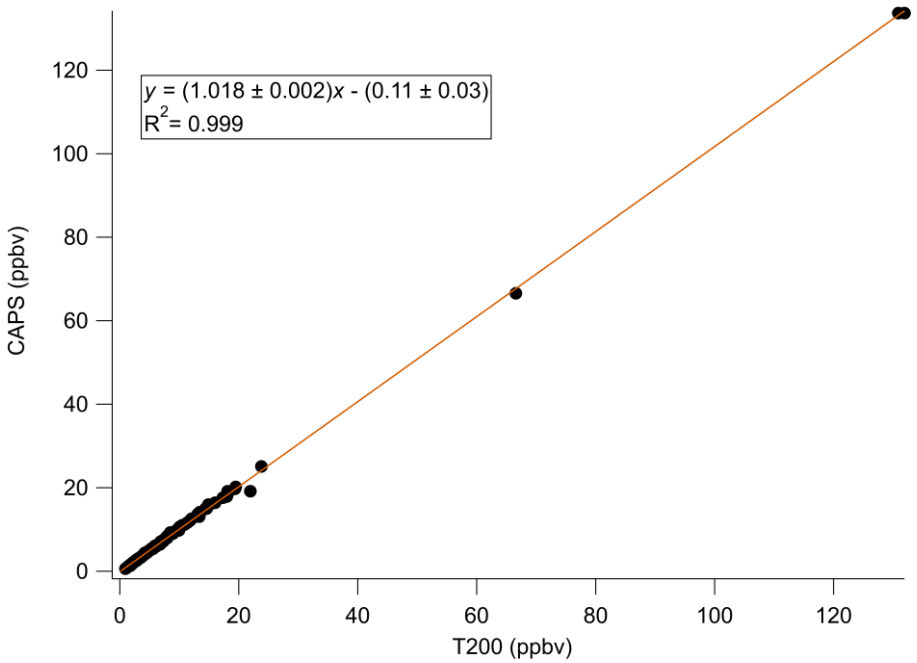

Figure A1 – Laboratory calibration curve for CAPS NO_2

(a)

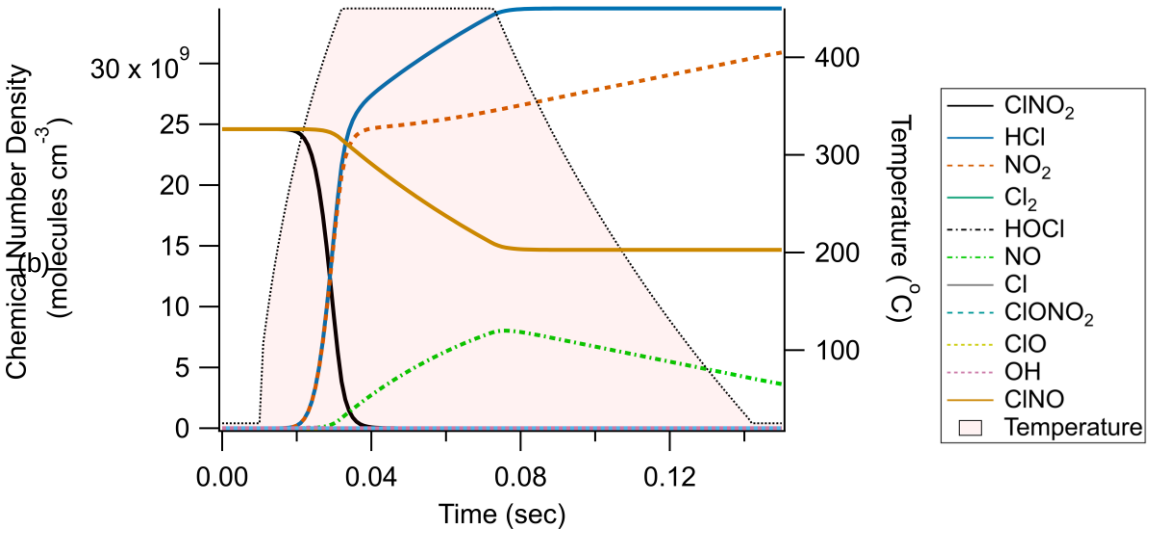

(b)

475

476 **Figure A2: Modelled effects of 2.46x 10^{10} (1 ppbv at 20°C) of ClNO.**

477

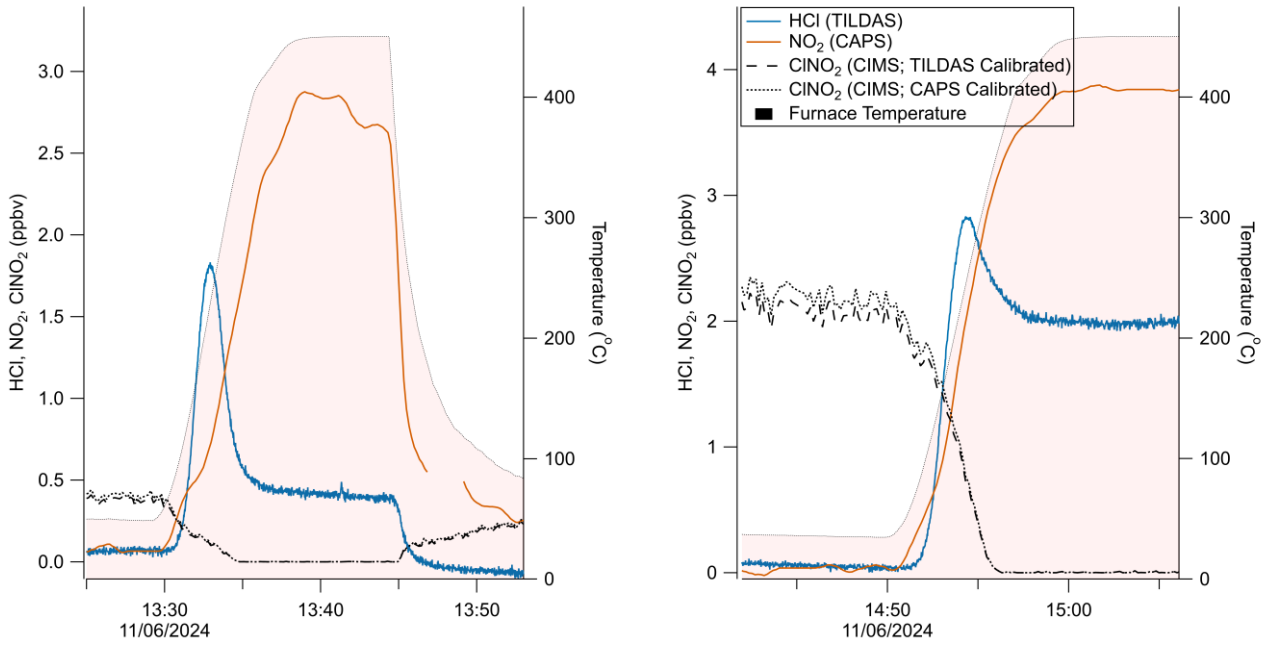

Figure A3 – a) Comparison plot of $ClNO_2$ observations with an apparent excess of NO_2 formed after aging/processing of the same slurry used for generating Fig. 3-4. (b) Additional comparison using a freshly made slurry. CIMS signal was calibrated using humidity-dependent calibration factors as presented in Fig. 5.

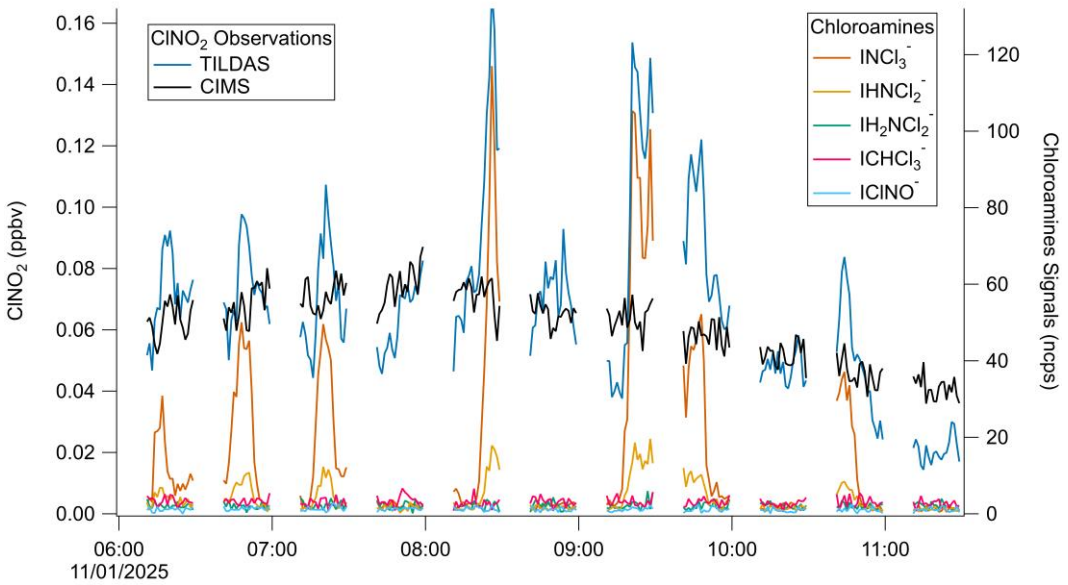

Figure A4 –Field data showing apparent coincident signal increases TILDAS-observed $ClNO_2$ with CIMS-observed chloramines, $IClNO^-$, and $ICHCl_3^-$ (uncalibrated).

Code availability

Code used for this analysis is available from the corresponding author on request.

Data availability

Data are available from the corresponding author on request.

Author contribution

PRV, MAR, SSB designed and performed proof-of-concept experiments to demonstrate potential of the method.
SCH, HRR, CD, TIY designed, built, and tested the HCl TILDAS at Aerodyne Research, Inc. SCH, HRR, CD, TIY, and PME designed initial laboratory experiments.
JWH and PME designed laboratory and field experiments, and JWH conducted laboratory and field experiments presented in this work.
LM, MDS, LJC provided support for laboratory use of CIMS. EM, TJB, HC provided support for field CIMS observations.
JWH prepared the manuscript, and all authors reviewed the manuscript.

Competing interests

The authors declare that they have no conflicts of interest.

Acknowledgements

The authors would also like to thank Abigail Mortimer for her glassblowing services, Stephen Andrews and Stuart Young for assistance with creating custom furnaces. Additionally, the authors thank William Drysdale and Katie Read for assistance with calibrating and using the York CAPS instrument. Further, the authors thank Michael Agnese and Michael Moore for TILDAS technical support.

Financial Support

This research has been supported by the European Research Council (H2020, grant no. ERC-StG 802685).

References

A. Angelucci, A., R. Crilley, L., Richardson, R., E. Valkenburg, T. S., S. Monks, P., M. Roberts, J., Sommariva, R., and C. VandenBoer, T.: Elevated levels of chloramines and chlorine detected near an indoor sports complex, Environmental Science: Processes & Impacts, 25, 304–313, https://doi.org/10.1039/D2EM00411A, 2023.

Anderson, L. and Fahey, D.: Studies with nitryl hypochlorite: Thermal dissociation rate and catalytic conversion to nitric oxide using an NO/O3 chemiluminescence detector, Journal of Physical Chemistry, 94, 644–652, 1990.

518 Atkinson, R., Baulch, D. L., Cox, R. A., Hampson, R. F., Jr., Kerr, J. A., and Troe, J.: Evaluated Kinetic and Photochemical
519 Data for Atmospheric Chemistry: Supplement IV. IUPAC Subcommittee on Gas Kinetic Data Evaluation for Atmospheric
520 Chemistry, Journal of Physical and Chemical Reference Data, 21, 1125, https://doi.org/10.1063/1.555918, 1992.

521 Atkinson, R., Baulch, D. L., Cox, R. A., Crowley, J. N., Hampson, R. F., Hynes, R. G., Jenkin, M. E., Rossi, M. J., and Troe,
522 J.: Evaluated kinetic and photochemical data for atmospheric chemistry: Volume I - gas phase reactions of O_x, HO_x, NO_x and
523 SO_x species, Atmospheric Chemistry and Physics, 4, 1461–1738, https://doi.org/10.5194/acp-4-1461-2004, 2004.

524 Atkinson, R., Baulch, D. L., Cox, R. A., Crowley, J. N., Hampson, R. F., Hynes, R. G., Jenkin, M. E., Rossi, M. J., Troe, J.,
525 and IUPAC Subcommittee: Evaluated kinetic and photochemical data for atmospheric chemistry: Volume II - gas phase
526 reactions of organic species, Atmospheric Chemistry and Physics, 6, 3625–4055, https://doi.org/10.5194/acp-6-3625-2006,
527 2006a.

528 Atkinson, R., Baulch, D. L., Cox, R. A., Crowley, J. N., Hampson, R. F., Hynes, R. G., Jenkin, M. E., Rossi, M. J., Troe, J.,
529 and IUPAC Subcommittee: Evaluated kinetic and photochemical data for atmospheric chemistry: Volume II - gas phase
530 reactions of organic species, Atmospheric Chemistry and Physics, 6, 3625–4055, https://doi.org/10.5194/acp-6-3625-2006,
531 2006b.

532 Atkinson, R., Baulch, D. L., Cox, R. A., Crowley, J. N., Hampson, R. F., Hynes, R. G., Jenkin, M. E., Rossi, M. J., and Troe,
533 J.: Evaluated kinetic and photochemical data for atmospheric chemistry: Volume III - gas phase reactions of inorganic
534 halogens, Atmospheric Chemistry and Physics, 7, 981–1191, https://doi.org/10.5194/acp-7-981-2007, 2007.

535 Atkinson, R., Baulch, D. L., Cox, R. A., Crowley, J. N., Hampson, R. F., Hynes, R. G., Jenkin, M. E., Rossi, M. J., Troe, J.,
536 and Wallington, T. J.: Evaluated kinetic and photochemical data for atmospheric chemistry: Volume IV – gas phase reactions
537 of organic halogen species, Atmospheric Chemistry and Physics, 8, 4141–4496, https://doi.org/10.5194/acp-8-4141-2008,
538 2008.

539 Bannan, T. J., Booth, A. M., Bacak, A., Muller, J. B. A., Leather, K. E., Le Breton, M., Jones, B., Young, D., Coe, H., Allan,
540 J., Visser, S., Slowik, J. G., Furger, M., Prévôt, A. S. H., Lee, J., Dunmore, R. E., Hopkins, J. R., Hamilton, J. F., Lewis, A.
541 C., Whalley, L. K., Sharp, T., Stone, D., Heard, D. E., Fleming, Z. L., Leigh, R., Shallcross, D. E., and Percival, C. J.: The
542 first UK measurements of nitryl chloride using a chemical ionization mass spectrometer in central London in the summer of
543 2012, and an investigation of the role of Cl atom oxidation, Journal of Geophysical Research: Atmospheres, 120, 5638–5657,
544 https://doi.org/10.1002/2014JD022629, 2015.

545 Baulch, D. L., Duxbury, J., Grant, S., and Montague, D. C.: Evaluated kinetic data for high temperature reactions. Volume 4.
546 Homogeneous gas phase reactions of halogen- and cyanide- containing species, J. Phys. Chem. Ref. Data, 10, 1–721, 1981.

547 Baulch, D. L., Cobos, C. J., Cox, R. A., Esser, C., Frank, P., Just, Th., Kerr, J. A., Pilling, M. J., Troe, J., Walker, R. W., and
548 Warnatz, J.: Evaluated Kinetic Data for Combustion Modelling, Journal of Physical and Chemical Reference Data, 21, 411,
549 https://doi.org/10.1063/1.555908, 1992.

550 Baulch, D. L., Cobos, C. J., Cox, R. A., Frank, P., Hayman, G., Just, Th., Kerr, J. A., Murrells, T., Pilling, M. J., Troe, J.,
551 Walker, R. W., and Warnatz, J.: Evaluated Kinetic Data for Combustion Modeling. Supplement I, Journal of Physical and
552 Chemical Reference Data, 23, 847–848, https://doi.org/10.1063/1.555953, 1994.

553 Bryukov, M. G., Slagle, I. R., and Knyazev, V. D.: Kinetics of Reactions of Cl Atoms with Methane and Chlorinated Methanes,
554 J. Phys. Chem. A, 106, 10532–10542, https://doi.org/10.1021/jp0257909, 2002.

555 Budisulistiorini, S. H., Li, X., Bairai, S. T., Renfro, J., Liu, Y., Liu, Y. J., McKinney, K. A., Martin, S. T., McNeill, V. F., Pye,
556 H. O. T., Nenes, A., Neff, M. E., Stone, E. A., Mueller, S., Knote, C., Shaw, S. L., Zhang, Z., Gold, A., and Surratt, J. D.:
557 Examining the effects of anthropogenic emissions on isoprene-derived secondary organic aerosol formation during the 2013
558 Southern Oxidant and Aerosol Study (SOAS) at the Look Rock, Tennessee ground site, Atmospheric Chemistry and Physics,
559 15, 8871–8888, https://doi.org/10.5194/acp-15-8871-2015, 2015.

560 Burkholder, J. B., Sander, S. P., Abbatt, J., Barker, J. R., Huie, R. E., Kolb, C. E., Kurylo, M. J., Orkin, V. L., Wilmouth, D.
561 M., and Wine, P. H.: Chemical Kinetics and Photochemical Data for Use in Atmospheric Studies, Evaluation No. 18, JPL
562 Publication 15-10., Jet Propulsion Laboratory, Pasadena, 2015.

563 Cantrell, C. A.: Technical Note: Review of methods for linear least-squares fitting of data and application to atmospheric
564 chemistry problems, Atmospheric Chemistry and Physics, 8, 5477–5487, https://doi.org/10.5194/acp-8-5477-2008, 2008.

565 Cohen, N. and Westberg, K. R.: Chemical Kinetic Data Sheets for High-Temperature Reactions. Part II, Journal of Physical
566 and Chemical Reference Data, 20, 1211–1311, https://doi.org/10.1063/1.555901, 1991.

567 Darwent, B. B.: Bond Dissociation Energies in Simple Molecules, U.S. National Bureau of Standards, 1970.

568 Day, D. A., Wooldridge, P. J., Dillon, M. B., Thornton, J. A., and Cohen, R. C.: A thermal dissociation laser-induced
569 fluorescence instrument for in situ detection of NO2, peroxy nitrates, alkyl nitrates, and HNO3, Journal of Geophysical
570 Research: Atmospheres, 107, ACH 4-1-ACH 4-14, https://doi.org/10.1029/2001JD000779, 2002.

571 Decker, Z. C. J., Novak, G. A., Aikin, K., Veres, P. R., Neuman, J. A., Bourgeois, I., Bui, T. P., Campuzano-Jost, P., Coggon,
572 M. M., Day, D. A., DiGangi, J. P., Diskin, G. S., Dollner, M., Franchin, A., Fredrickson, C. D., Froyd, K. D., Gkatzelis, G. I.,
573 Guo, H., Hall, S. R., Halliday, H., Hayden, K., Holmes, C. D., Jimenez, J. L., Kupc, A., Lindaas, J., Middlebrook, A. M.,
574 Moore, R. H., Nault, B. A., Nowak, J. B., Pagonis, D., Palm, B. B., Peischl, J., Piel, F. M., Rickly, P. S., Robinson, M. A.,
575 Rollins, A. W., Ryerson, T. B., Schill, G. P., Sekimoto, K., Thompson, C. R., Thornhill, K. L., Thornton, J. A., Ullmann, K.,
576 Warneke, C., Washenfelder, R. A., Weinzierl, B., Wiggins, E. B., Williamson, C. J., Winstead, E. L., Wisthaler, A., Womack,
577 C. C., and Brown, S. S.: Airborne Observations Constrain Heterogeneous Nitrogen and Halogen Chemistry on Tropospheric
578 and Stratospheric Biomass Burning Aerosol, Geophysical Research Letters, 51, e2023GL107273,
579 https://doi.org/10.1029/2023GL107273, 2024.

580 Driscoll, C. T., Mason, R. P., Chan, H. M., Jacob, D. J., and Pirrone, N.: Mercury as a Global Pollutant: Sources, Pathways,
581 and Effects, Environ. Sci. Technol., 47, 4967–4983, https://doi.org/10.1021/es305071v, 2013.

582 Frenzel, A., Scheer, V., Sikorski, R., George, Ch., Behnke, W., and Zetzsch, C.: Heterogeneous Interconversion Reactions of
583 BrNO2, ClNO2, Br2, and Cl2, J. Phys. Chem. A, 102, 1329–1337, https://doi.org/10.1021/jp973044b, 1998.

584 Furlani, T. C., Veres, P. R., Dawe, K. E. R., Neuman, J. A., Brown, S. S., VandenBoer, T. C., and Young, C. J.: Validation of
585 a new cavity ring-down spectrometer for measuring tropospheric gaseous hydrogen chloride, Atmospheric Measurement
586 Techniques, 14, 5859–5871, https://doi.org/10.5194/amt-14-5859-2021, 2021.

587 Guelachvili, G., Niay, P., and Bernage, P.: Infrared bands of HCl and DCl by Fourier transform spectroscopy: Dunham
588 coefficients for HCl, DCl, and TCl, Journal of Molecular Spectroscopy, 85, 271–281, https://doi.org/10.1016/0022-
589 2852(81)90200-9, 1981.

590 Hagen, C. L., Lee, B. C., Franka, I. S., Rath, J. L., VandenBoer, T. C., Roberts, J. M., Brown, S. S., and Yalin, A. P.: Cavity
591 ring-down spectroscopy sensor for detection of hydrogen chloride, Atmospheric Measurement Techniques, 7, 345–357,
592 https://doi.org/10.5194/amt-7-345-2014, 2014.

593 Halfacre, J. W. and Simpson, W. R.: Polar Tropospheric Ozone Depletion Events, in: Chemistry in the Cryosphere, vol.
594 Volume 3, WORLD SCIENTIFIC, 411–452, https://doi.org/10.1142/9789811230134_0008, 2022.

595 Halfacre, J. W., Stewart, J., Herndon, S. C., Roscioli, J. R., Dyroff, C., Yacovitch, T. I., Flynn, M., Andrews, S. J., Brown, S.
596 S., Veres, P. R., and Edwards, P. M.: Using tunable infrared laser direct absorption spectroscopy for ambient hydrogen chloride
597 detection: HCl-TILDAS, Atmospheric Measurement Techniques, 16, 1407–1429, https://doi.org/10.5194/amt-16-1407-2023,
598 2023.

599 Heimerl, J. M. and Coffee, T. P.: The unimolecular ozone decomposition reaction, Combustion and Flame, 35, 117–123,
600 https://doi.org/10.1016/0010-2180(79)90015-4, 1979.

601 Hellén, H., Kouznetsov, R., Kraft, K., Seppälä, J., Vestenius, M., Jalkanen, J.-P., Laakso, L., and Hakola, H.: Shipping and
602 algae emissions have a major impact on ambient air mixing ratios of non-methane hydrocarbons (NMHCs) and methanethiol
603 on Utö Island in the Baltic Sea, Atmospheric Chemistry and Physics, 24, 4717–4731, https://doi.org/10.5194/acp-24-4717-
604 2024, 2024.

605 Huffman, J. A., Docherty, K. S., Aiken, A. C., Cubison, M. J., Ulbrich, I. M., DeCarlo, P. F., Sueper, D., Jayne, J. T., Worsnop,
606 D. R., Ziemann, P. J., and Jimenez, J. L.: Chemically-resolved aerosol volatility measurements from two megacity field studies,
607 Atmos. Chem. Phys., 9, 7161–7182, https://doi.org/10.5194/acp-9-7161-2009, 2009.

608 Ianni, J. C.: - A comparison of the Bader-Deuflhard and the Cash-Karp Runge-Kutta integrators for the GRI-MECH 3.0 model
609 based on the chemical kinetics code Kintecus, in: Computational Fluid and Solid Mechanics 2003, edited by: Bathe, K. J.,
610 Elsevier Science Ltd, Oxford, 1368–1372, https://doi.org/10.1016/B978-008044046-0.50335-3, 2003.

Ianni, J. C.: Kintecus, 2022.

Jaeglé, L., Shah, V., Thornton, J. A., Lopez-Hilfiker, F. D., Lee, B. H., McDuffie, E. E., Fibiger, D., Brown, S. S., Veres, P., Sparks, T. L., Ebben, C. J., Wooldridge, P. J., Kenagy, H. S., Cohen, R. C., Weinheimer, A. J., Campos, T. L., Montzka, D. D., Digangi, J. P., Wolfe, G. M., Hanisco, T., Schroder, J. C., Campuzano-Jost, P., Day, D. A., Jimenez, J. L., Sullivan, A. P., Guo, H., and Weber, R. J.: Nitrogen Oxides Emissions, Chemistry, Deposition, and Export Over the Northeast United States During the WINTER Aircraft Campaign, Journal of Geophysical Research: Atmospheres, 123, 12,368-12,393, https://doi.org/10.1029/2018JD029133, 2018.

Ji, Y., Huey, L. G., Tanner, D. J., Lee, Y. R., Veres, P. R., Neuman, J. A., Wang, Y., and Wang, X.: A vacuum ultraviolet ion source (VUV-IS) for iodide–chemical ionization mass spectrometry: a substitute for radioactive ion sources, Atmospheric Measurement Techniques, 13, 3683–3696, https://doi.org/10.5194/amt-13-3683-2020, 2020.

Kercher, J. P., Riedel, T. P., and Thornton, J. A.: Chlorine activation by N_2O_5: simultaneous, in situ detection of $ClNO_2$ and N_2O_5 by chemical ionization mass spectrometry, Atmospheric Measurement Techniques, 2, 193–204, https://doi.org/10.5194/amt-2-193-2009, 2009.

Le Breton, M., Hallquist, Å. M., Pathak, R. K., Simpson, D., Wang, Y., Johansson, J., Zheng, J., Yang, Y., Shang, D., Wang, H., Liu, Q., Chan, C., Wang, T., Bannan, T. J., Priestley, M., Percival, C. J., Shallcross, D. E., Lu, K., Guo, S., Hu, M., and Hallquist, M.: Chlorine oxidation of VOCs at a semi-rural site in Beijing: significant chlorine liberation from $ClNO_2$ and subsequent gas- and particle-phase Cl–VOC production, Atmospheric Chemistry and Physics, 18, 13013–13030, https://doi.org/10.5194/acp-18-13013-2018, 2018.

Lee, B. H., Lopez-Hilfiker, F. D., Mohr, C., Kurtén, T., Worsnop, D. R., and Thornton, J. A.: An Iodide-Adduct High-Resolution Time-of-Flight Chemical-Ionization Mass Spectrometer: Application to Atmospheric Inorganic and Organic Compounds, Environ. Sci. Technol., 48, 6309–6317, https://doi.org/10.1021/es500362a, 2014.

Lee, B. H., Lopez-Hilfiker, F. D., Schroder, J. C., Campuzano-Jost, P., Jimenez, J. L., McDuffie, E. E., Fibiger, D. L., Veres, P. R., Brown, S. S., Campos, T. L., Weinheimer, A. J., Flocke, F. F., Norris, G., O'Mara, K., Green, J. R., Fiddler, M. N., Bililign, S., Shah, V., Jaeglé, L., and Thornton, J. A.: Airborne Observations of Reactive Inorganic Chlorine and Bromine Species in the Exhaust of Coal-Fired Power Plants, Journal of Geophysical Research: Atmospheres, 123, 11,225-11,237, https://doi.org/10.1029/2018JD029284, 2018a.

Lee, B. H., Lopez-Hilfiker, F. D., Veres, P. R., McDuffie, E. E., Fibiger, D. L., Sparks, T. L., Ebben, C. J., Green, J. R., Schroder, J. C., Campuzano-Jost, P., Iyer, S., D'Ambro, E. L., Schobesberger, S., Brown, S. S., Wooldridge, P. J., Cohen, R. C., Fiddler, M. N., Bililign, S., Jimenez, J. L., Kurtén, T., Weinheimer, A. J., Jaegle, L., and Thornton, J. A.: Flight Deployment of a High-Resolution Time-of-Flight Chemical Ionization Mass Spectrometer: Observations of Reactive Halogen and Nitrogen Oxide Species, Journal of Geophysical Research: Atmospheres, 123, 7670–7686, https://doi.org/10.1029/2017JD028082, 2018b.

Liao, J., Huey, L. G., Liu, Z., Tanner, D. J., Cantrell, C. A., Orlando, J. J., Flocke, F. M., Shepson, P. B., Weinheimer, A. J., Hall, S. R., Ullmann, K., Beine, H. J., Wang, Y., Ingall, E. D., Stephens, C. R., Hornbrook, R. S., Apel, E. C., Riemer, D., Fried, A., Mauldin Iii, R. L., Smith, J. N., Staebler, R. M., Neuman, J. A., and Nowak, J. B.: High levels of molecular chlorine in the Arctic atmosphere, Nature Geosci, 7, 91–94, https://doi.org/10.1038/ngeo2046, 2014.

Liu, X., Qu, H., Huey, L. G., Wang, Y., Sjostedt, S., Zeng, L., Lu, K., Wu, Y., Hu, M., Shao, M., Zhu, T., and Zhang, Y.: High Levels of Daytime Molecular Chlorine and Nitryl Chloride at a Rural Site on the North China Plain, Environ. Sci. Technol., 51, 9588–9595, https://doi.org/10.1021/acs.est.7b03039, 2017.

Macken, K. V. and Sidebottom, H. W.: The reactions of methyl radicals with chloromethanes, International Journal of Chemical Kinetics, 11, 511–527, https://doi.org/10.1002/kin.550110505, 1979.

Mahmud, K., Kim, J. S., and Fontijn, A.: A high-temperature photochemical kinetics study of the oxygen atom+ hydrogen chloride reaction from 350 to 1480 K, Journal of Physical Chemistry, 94, 2994–2998, 1990.

Manion, J. A., Huie, R. E., Levin, R. D., Burgess Jr., D. R., Orkin, V. L., Tsang, W., McGivern, W. S., Hudgens, J. W., Knyazev, V. D., Atkinson, D. B., Chai, E., Tereza, A. M., Lin, C.-Y., Allison, T. C., Mallard, W. G., Westley, F., Herron, J. T., Hampson, R. F., and Frizzell, D. H.: NIST Chemical Kinetics Database (NIST Standard Reference Database 17, Version 7.0 (Web Version), Release 1.6.8, Data version 2015.09), 2015.

McManus, J. B., Zahniser, M. S., and Nelson, D. D.: Dual quantum cascade laser trace gas instrument with astigmatic Herriott cell at high pass number, Appl. Opt., 50, A74, https://doi.org/10.1364/AO.50.000A74, 2011.

McManus, J. B., Zahniser, M. S., Nelson, D. D., Shorter, J. H., Herndon, S. C., Jervis, D., Agnese, M., McGovern, R., Yacovitch, T. I., and Roscioli, J. R.: Recent progress in laser-based trace gas instruments: performance and noise analysis, Appl. Phys. B, 119, 203–218, https://doi.org/10.1007/s00340-015-6033-0, 2015.

McNamara, S. M., Kolesar, K. R., Wang, S., Kirpes, R. M., May, N. W., Gunsch, M. J., Cook, R. D., Fuentes, J. D., Hornbrook, R. S., Apel, E. C., China, S., Laskin, A., and Pratt, K. A.: Observation of Road Salt Aerosol Driving Inland Wintertime Atmospheric Chlorine Chemistry, ACS Cent. Sci., 6, 684–694, https://doi.org/10.1021/acscentsci.9b00994, 2020.

Mielke, L. H., Furgeson, A., and Osthoff, H. D.: Observation of $ClNO_2$ in a Mid-Continental Urban Environment, Environ. Sci. Technol., 45, 8889–8896, https://doi.org/10.1021/es201955u, 2011.

Moravek, A., VandenBoer, T. C., Finewax, Z., Pagonis, D., Nault, B. A., Brown, W. L., Day, D. A., Handschy, A. V., Stark, H., Ziemann, P., Jimenez, J. L., de Gouw, J. A., and Young, C. J.: Reactive Chlorine Emissions from Cleaning and Reactive Nitrogen Chemistry in an Indoor Athletic Facility, Environ. Sci. Technol., 56, 15408–15416, https://doi.org/10.1021/acs.est.2c04622, 2022.

Orlando, J. J., Tyndall, G. S., Apel, E. C., Riemer, D. D., and Paulson, S. E.: Rate coefficients and mechanisms of the reaction of cl-atoms with a series of unsaturated hydrocarbons under atmospheric conditions, International Journal of Chemical Kinetics, 35, 334–353, https://doi.org/10.1002/kin.10135, 2003.

Osthoff, H. D., Roberts, J. M., Ravishankara, A. R., Williams, E. J., Lerner, B. M., Sommariva, R., Bates, T. S., Coffman, D., Quinn, P. K., Dibb, J. E., Stark, H., Burkholder, J. B., Talukdar, R. K., Meagher, J., Fehsenfeld, F. C., and Brown, S. S.: High levels of nitryl chloride in the polluted subtropical marine boundary layer, Nature Geoscience, 1, 324–328, https://doi.org/10.1038/ngeo177, 2008.

Phillips, G. J., Tang, M. J., Thieser, J., Brickwedde, B., Schuster, G., Bohn, B., Lelieveld, J., and Crowley, J. N.: Significant concentrations of nitryl chloride observed in rural continental Europe associated with the influence of sea salt chloride and anthropogenic emissions, Geophysical Research Letters, 39, https://doi.org/10.1029/2012GL051912, 2012.

R Core Team: R: A language and environment for statistical computing., 2021.

Raff, J. D., Njegic, B., Chang, W. L., Gordon, M. S., Dabdub, D., Gerber, R. B., and Finlayson-Pitts, B. J.: Chlorine activation indoors and outdoors via surface-mediated reactions of nitrogen oxides with hydrogen chloride, Proceedings of the National Academy of Sciences, 106, 13647–13654, https://doi.org/10.1073/pnas.0904195106, 2009.

Riedel, T. P., Bertram, T. H., Crisp, T. A., Williams, E. J., Lerner, B. M., Vlasenko, A., Li, S.-M., Gilman, J., de Gouw, J., Bon, D. M., Wagner, N. L., Brown, S. S., and Thornton, J. A.: Nitryl Chloride and Molecular Chlorine in the Coastal Marine Boundary Layer, Environ. Sci. Technol., 46, 10463–10470, https://doi.org/10.1021/es204632r, 2012.

Riedel, T. P., Wagner, N. L., Dubé, W. P., Middlebrook, A. M., Young, C. J., Öztürk, F., Bahreini, R., VandenBoer, T. C., Wolfe, D. E., Williams, E. J., Roberts, J. M., Brown, S. S., and Thornton, J. A.: Chlorine activation within urban or power plant plumes: Vertically resolved $ClNO_2$ and Cl_2 measurements from a tall tower in a polluted continental setting, Journal of Geophysical Research: Atmospheres, 118, 8702–8715, https://doi.org/10.1002/jgrd.50637, 2013.

Riva, M., Pospisilova, V., Frege, C., Perrier, S., Bansal, P., Jorga, S., Sturm, P., Thornton, J. A., Rohner, U., and Lopez-Hilfiker, F.: Evaluation of a reduced-pressure chemical ion reactor utilizing adduct ionization for the detection of gaseous organic and inorganic species, Atmospheric Measurement Techniques, 17, 5887–5901, https://doi.org/10.5194/amt-17-5887-2024, 2024.

Robinson, M. A., Neuman, J. A., Huey, L. G., Roberts, J. M., Brown, S. S., and Veres, P. R.: Temperature-dependent sensitivity of iodide chemical ionization mass spectrometers, Atmospheric Measurement Techniques, 15, 4295–4305, https://doi.org/10.5194/amt-15-4295-2022, 2022.

Roscioli, J. R., Zahniser, M. S., Nelson, D. D., Herndon, S. C., and Kolb, C. E.: New Approaches to Measuring Sticky Molecules: Improvement of Instrumental Response Times Using Active Passivation, J. Phys. Chem. A, 120, 1347–1357, https://doi.org/10.1021/acs.jpca.5b04395, 2016.

Sarwar, G., Simon, H., Bhave, P., and Yarwood, G.: Examining the impact of heterogeneous nitryl chloride production on air quality across the United States, Atmospheric Chemistry and Physics, 12, 6455–6473, https://doi.org/10.5194/acp-12-6455-2012, 2012.

Sarwar, G., Simon, H., Xing, J., and Mathur, R.: Importance of tropospheric ClNO2 chemistry across the Northern Hemisphere, Geophysical Research Letters, 41, 4050–4058, https://doi.org/10.1002/2014GL059962, 2014.

Simon, H., Kimura, Y., McGaughey, G., Allen, D. T., Brown, S. S., Osthoff, H. D., Roberts, J. M., Byun, D., and Lee, D.: Modeling the impact of $ClNO_2$ on ozone formation in the Houston area, J. Geophys. Res., 114, D00F03, https://doi.org/10.1029/2008JD010732, 2009.

Simpson, W. R., Brown, S. S., Saiz-Lopez, A., Thornton, J. A., and von Glasow, R.: Tropospheric Halogen Chemistry: Sources, Cycling, and Impacts, Chem. Rev., 115, 4035–4062, https://doi.org/10.1021/cr5006638, 2015.

Sommariva, R., Hollis, L. D. J., Sherwen, T., Baker, A. R., Ball, S. M., Bandy, B. J., Bell, T. G., Chowdhury, M. N., Cordell, R. L., Evans, M. J., Lee, J. D., Reed, C., Reeves, C. E., Roberts, J. M., Yang, M., and Monks, P. S.: Seasonal and geographical variability of nitryl chloride and its precursors in Northern Europe, Atmospheric Science Letters, 19, e844, https://doi.org/10.1002/asl.844, 2018.

Srinivasan, N. K., Su, M.-C., Sutherland, J. W., and Michael, J. V.: Reflected Shock Tube Studies of High-Temperature Rate Constants for OH + CH4 → CH3 + H2O and CH3 + NO2 → CH3O + NO, J. Phys. Chem. A, 109, 1857–1863, https://doi.org/10.1021/jp040679j, 2005.

Tan, Z., Fuchs, H., Hofzumahaus, A., Bloss, W. J., Bohn, B., Cho, C., Hohaus, T., Holland, F., Lakshmisha, C., Liu, L., Monks, P. S., Novelli, A., Niether, D., Rohrer, F., Tillmann, R., Valkenburg, T. S. E., Vardhan, V., Kiendler-Scharr, A., Wahner, A., and Sommariva, R.: Seasonal variation in nitryl chloride and its relation to gas-phase precursors during the JULIAC campaign in Germany, Atmospheric Chemistry and Physics, 22, 13137–13152, https://doi.org/10.5194/acp-22-13137-2022, 2022.

Thaler, R. D., Mielke, L. H., and Osthoff, H. D.: Quantification of Nitryl Chloride at Part Per Trillion Mixing Ratios by Thermal Dissociation Cavity Ring-Down Spectroscopy, Anal. Chem., 83, 2761–2766, https://doi.org/10.1021/ac200055z, 2011.

Tham, Y. J., Wang, Z., Li, Q., Yun, H., Wang, W., Wang, X., Xue, L., Lu, K., Ma, N., Bohn, B., Li, X., Kecorius, S., Größ, J., Shao, M., Wiedensohler, A., Zhang, Y., and Wang, T.: Significant concentrations of nitryl chloride sustained in the morning: investigations of the causes and impacts on ozone production in a polluted region of northern China, Atmospheric Chemistry and Physics, 16, 14959–14977, https://doi.org/10.5194/acp-16-14959-2016, 2016.

Tham, Y. J., Wang, Z., Li, Q., Wang, W., Wang, X., Lu, K., Ma, N., Yan, C., Kecorius, S., Wiedensohler, A., Zhang, Y., and Wang, T.: Heterogeneous N_2O_5 uptake coefficient and production yield of $ClNO_2$ in polluted northern China: roles of aerosol water content and chemical composition, Atmospheric Chemistry and Physics, 18, 13155–13171, https://doi.org/10.5194/acp-18-13155-2018, 2018.

Thornton, J. A., Kercher, J. P., Riedel, T. P., Wagner, N. L., Cozic, J., Holloway, J. S., Dubé, W. P., Wolfe, G. M., Quinn, P. K., Middlebrook, A. M., Alexander, B., and Brown, S. S.: A large atomic chlorine source inferred from mid-continental reactive nitrogen chemistry, Nature, 464, 271–274, https://doi.org/10.1038/nature08905, 2010.

Tripathi, N., Sahu, L. K., Patel, K., Kumar, A., and Yadav, R.: Ambient air characteristics of biogenic volatile organic compounds at a tropical evergreen forest site in Central Western Ghats of India, J Atmos Chem, 78, 139–159, https://doi.org/10.1007/s10874-021-09415-y, 2021.

Troe, J.: Refined Representation of Falloff Curves for the Reaction HO + NO2 + N2 → (HONO2, HOONO) + N2, J. Phys. Chem. A, 116, 6387–6393, https://doi.org/10.1021/jp212095n, 2012.

Wagner, N. L., Riedel, T. P., Young, C. J., Bahreini, R., Brock, C. A., Dubé, W. P., Kim, S., Middlebrook, A. M., Öztürk, F., Roberts, J. M., Russo, R., Sive, B., Swarthout, R., Thornton, J. A., VandenBoer, T. C., Zhou, Y., and Brown, S. S.: N_2O_5 uptake coefficients and nocturnal NO_2 removal rates determined from ambient wintertime measurements, Journal of Geophysical Research: Atmospheres, 118, 9331–9350, https://doi.org/10.1002/jgrd.50653, 2013.

Wallington, T., Ammann, M., Cox, R. A., Crowley, J. N., Herrmann, H., Jenkin, M. E., McNeill, V. F., Mellouki, A. W., and Troe, J.: Evaluated Kinetic Data for Atmospheric Chemistry, 2021.

Wang, C., Liggio, J., Wentzell, J. J. B., Jorga, S., Folkerson, A., and Abbatt, J. P. D.: Chloramines as an important photochemical source of chlorine atoms in the urban atmosphere, Proceedings of the National Academy of Sciences, 120, e2220889120, https://doi.org/10.1073/pnas.2220889120, 2023.

Wang, H., Yuan, B., Zheng, E., Zhang, X., Wang, J., Lu, K., Ye, C., Yang, L., Huang, S., Hu, W., Yang, S., Peng, Y., Qi, J., Wang, S., He, X., Chen, Y., Li, T., Wang, W., Huangfu, Y., Li, X., Cai, M., Wang, X., and Shao, M.: Formation and impacts of nitryl chloride in Pearl River Delta, Atmospheric Chemistry and Physics, 22, 14837–14858, https://doi.org/10.5194/acp-22-14837-2022, 2022.

Wang, T., Tham, Y. J., Xue, L., Li, Q., Zha, Q., Wang, Z., Poon, S. C. N., Dubé, W. P., Blake, D. R., Louie, P. K. K., Luk, C. W. Y., Tsui, W., and Brown, S. S.: Observations of nitryl chloride and modeling its source and effect on ozone in the planetary boundary layer of southern China: ClNO 2 IN PBL OF CHINA, J. Geophys. Res. Atmos., 121, 2476–2489, https://doi.org/10.1002/2015JD024556, 2016.

Wang, X., Jacob, D. J., Eastham, S. D., Sulprizio, M. P., Zhu, L., Chen, Q., Alexander, B., Sherwen, T., Evans, M. J., Lee, B. H., Haskins, J. D., Lopez-Hilfiker, F. D., Thornton, J. A., Huey, G. L., and Liao, H.: The role of chlorine in global tropospheric chemistry, Atmospheric Chemistry and Physics, 19, 3981–4003, https://doi.org/10.5194/acp-19-3981-2019, 2019.

Wang, X., Jacob, D. J., Downs, W., Zhai, S., Zhu, L., Shah, V., Holmes, C. D., Sherwen, T., Alexander, B., Evans, M. J., Eastham, S. D., Neuman, J. A., Veres, P. R., Koenig, T. K., Volkamer, R., Huey, L. G., Bannan, T. J., Percival, C. J., Lee, B. H., and Thornton, J. A.: Global tropospheric halogen (Cl, Br, I) chemistry and its impact on oxidants, Atmospheric Chemistry and Physics, 21, 13973–13996, https://doi.org/10.5194/acp-21-13973-2021, 2021.

Wang, Z., Wang, W., Tham, Y. J., Li, Q., Wang, H., Wen, L., Wang, X., and Wang, T.: Fast heterogeneous N_2O_5 uptake and $ClNO_2$ production in power plant and industrial plumes observed in the nocturnal residual layer over the North China Plain, Atmospheric Chemistry and Physics, 17, 12361–12378, https://doi.org/10.5194/acp-17-12361-2017, 2017.

Weissman, M. and Benson, S. W.: Heat of formation of the CHCl2 radical. Bond dissociation energies in chloromethanes and chloroethanes, J. Phys. Chem., 87, 243–244, https://doi.org/10.1021/j100225a014, 1983.

Westenberg, A. A. and deHaas, N.: Rates of H+CH3X reactions, The Journal of Chemical Physics, 62, 3321–3325, https://doi.org/10.1063/1.430925, 1975.

Wilkerson, J., Sayres, D. S., Smith, J. B., Allen, N., Rivero, M., Greenberg, M., Martin, T., and Anderson, J. G.: In situ observations of stratospheric HCl using three-mirror integrated cavity output spectroscopy, Atmospheric Measurement Techniques Discussions, 1–38, https://doi.org/10.5194/amt-2021-6, 2021.

World Meteorological Organization: Scientific Assessment of Ozone Depletion: 2022, WMO, Geneva, 2022.

Xia, M., Peng, X., Wang, W., Yu, C., Sun, P., Li, Y., Liu, Y., Xu, Z., Wang, Z., Xu, Z., Nie, W., Ding, A., and Wang, T.: Significant production of $ClNO_2$ and possible source of Cl_2 from N_2O_5 uptake at a suburban site in eastern China, Atmospheric Chemistry and Physics, 20, 6147–6158, https://doi.org/10.5194/acp-20-6147-2020, 2020.

Xiao, F., Sasi, P. C., Yao, B., Kubátová, A., Golovko, S. A., Golovko, M. Y., and Soli, D.: Thermal Stability and Decomposition of Perfluoroalkyl Substances on Spent Granular Activated Carbon, Environ. Sci. Technol. Lett., 7, 343–350, https://doi.org/10.1021/acs.estlett.0c00114, 2020.

Ye, C., Yuan, B., Lin, Y., Wang, Z., Hu, W., Li, T., Chen, W., Wu, C., Wang, C., Huang, S., Qi, J., Wang, B., Wang, C., Song, W., Wang, X., Zheng, E., Krechmer, J. E., Ye, P., Zhang, Z., Wang, X., Worsnop, D. R., and Shao, M.: Chemical characterization of oxygenated organic compounds in the gas phase and particle phase using iodide CIMS with FIGAERO in urban air, Atmospheric Chemistry and Physics, 21, 8455–8478, https://doi.org/10.5194/acp-21-8455-2021, 2021.

Young, C. J., Washenfelder, R. A., Roberts, J. M., Mielke, L. H., Osthoff, H. D., Tsai, C., Pikelnaya, O., Stutz, J., Veres, P. R., Cochran, A. K., VandenBoer, T. C., Flynn, J., Grossberg, N., Haman, C. L., Lefer, B., Stark, H., Graus, M., de Gouw, J., Gilman, J. B., Kuster, W. C., and Brown, S. S.: Vertically Resolved Measurements of Nighttime Radical Reservoirs in Los Angeles and Their Contribution to the Urban Radical Budget, Environ. Sci. Technol., 46, 10965–10973, https://doi.org/10.1021/es302206a, 2012.

Yu, C., Wang, Z., Xia, M., Fu, X., Wang, W., Tham, Y. J., Chen, T., Zheng, P., Li, H., Shan, Y., Wang, X., Xue, L., Zhou, Y., Yue, D., Ou, Y., Gao, J., Lu, K., Brown, S. S., Zhang, Y., and Wang, T.: Heterogeneous N_2O_5 reactions on atmospheric

795 aerosols at four Chinese sites: improving model representation of uptake parameters, Atmospheric Chemistry and Physics, 20,
796 4367–4378, https://doi.org/10.5194/acp-20-4367-2020, 2020.

797 Zhou, W., Zhao, J., Ouyang, B., Mehra, A., Xu, W., Wang, Y., Bannan, T. J., Worrall, S. D., Priestley, M., Bacak, A., Chen,
798 Q., Xie, C., Wang, Q., Wang, J., Du, W., Zhang, Y., Ge, X., Ye, P., Lee, J. D., Fu, P., Wang, Z., Worsnop, D., Jones, R.,
799 Percival, C. J., Coe, H., and Sun, Y.: Production of N_2O_5 and $ClNO_2$ in summer in urban Beijing, China, Atmospheric
800 Chemistry and Physics, 18, 11581–11597, https://doi.org/10.5194/acp-18-11581-2018, 2018.

801